INSECT POWERED MICRO AIR VEHICLES AND CENTIMETER SCALE HIGH ENERGY DENSITY PNEUMATIC SOURCES

A Dissertation

Presented to the Faculty of the Graduate School

of Cornell University

in Partial Fulfillment of the Requirements for the Degree of

Doctor of Philosophy

by

Venkata Siva Prasad Pulla

January 2012

INSECT POWERED MICRO AIR VEHICLES AND CENTIMETER SCALE HIGH ENERGY DENSITY PNEUMATIC SOURCES

Venkata Siva Prasad Pulla, Ph.D.

Cornell University 2012

The flight times of traditional Micro-Air-Vehicles (MAVs) are limited by low energy density of batteries at small scale. On the other hand insects outperform MAVs in terms of flight time due to the higher energy density of carbohydrates and fat. Some of the most successful flapping wing MAVs have continuous flight time of only about 15 minutes, while some insects can have continuous flight times as high as three hours. Motivated by this, we have worked towards realization of insect powered MAVs. This dissertation presents successful navigation of moths, using light-weight and low-power actuators, demonstrating insect powered MAVs (IPMAV) for the first time. These MAVs can fly for long periods of time, consuming only a small fraction (1%) of power compared to purely mechanical MAVs. Untethered flight control of Balloon enabled IPMAVs was achieved using force based techniques. Flight control distances of over 1-km and flight times of 40 minutes were achieved. This dissertation also reports the first use of carbon-fiber composite Centimeter-Scale High Pressure-Vessel (CSHPV) applied to MEMS actuators. We present the design, fabrication and testing of MEMS compatible CSHPV and valves with pneumatic energy densities exceeding those of the traditional Lithium battery and electromechanical actuator combination. The pneumatic power sources can provide direct mechanical power to move mechanical elements, enabling pathway for highly efficient operation. The 1-2 cc pressure vessels with burst pressures as high as 3250 bar

were achieved corresponding to an energy density of 20.5 Wh/Kg, comparable to 50 Wh/Kg of Lithium batteries with similar volumes. A novel microfluidic interface to the CSHPV was realized using glass capillaries that provide high fluidic resistance at high pressures. Electromagnetic coil valves were fabricated to control CO_2 flow from 10-20 micron diameter glass capillaries that could actuate surface micromachined polysilicon micromotors.

BIOGRAPHICAL SKETCH

Siva was born in Visakhapatnam, Andhra Pradesh, India. He graduated with a Bachelors degree in Mechanical Engineering from the Indian Institute of Technology Madras, India in 2004. In the same year, he began pursuing his Ph.D. degree in Cornell University. He has been with the SonicMEMS lab pursing Ph.D. in Electrical Engineering under the guidance of Dr. Amit Lal since Spring of 2005.

To my parents, my brother and family.

ACKNOWLEDGEMENTS

The past few years at Cornell have been the most exciting and professionally formative years of my life. I would like to acknowledge the outstanding people that enabled and enriched this experience. I am grateful to Professor Amit Lal for the opportunity to conduct research in the exciting field of Insect MEMS. His enthusiasm for constantly exploring new ideas, optimism in the face of seemingly insurmountable technological hurdles, and creativity in solving those problems have strongly influenced my years in the Ph.D. program. I cannot thank him enough for all the confidence he has placed in me, and the freedom he has given me throughout my Ph.D. I would like to thank Committee members Professor Sunil Bhave, for all the great discussions and words of encouragement and Professor Jane Wang for helpful discussions. I am also truly thankful for the outstanding colleagues I have worked with during my Ph.D., Shankar and Serhan who will be an inspiration to me in the years to come. Of course, needless to say, I would like to thanks the rest of the SonicMEMS members and for all the good times.

TABLE OF CONTENTS

LIST OF TABLES

LIST OF FIGURES

CHAPTER 1

SUITABILITY OF INSECTS AS MICRO AIR VEHICLES (MAVS)

1.1 Introduction

Micro-Air-Vehicles (MAVs) are unmanned aerial vehicles that have a wing span on the order of few centimeters and are capable of carrying pay load of a few grams (Figure 1.1). MAVs provide the benefit of stealth, combined with maneuverability making them ideal for operations that involve considerable risk to human beings. Applications requiring such compactness and agility include but are not limited to search and rescue, military or law enforcement surveillance, chemical or biological agent detection or reconnaissance in confined spaces [1, 2]. Figure 1.2 A shows the scaling of the aerodynamic operation of the MAV. The Reynolds number (Re) is defined as:

$$Re = \frac{\rho U D}{\mu} \tag{1.1}$$

where ρ is the density of air, U is the forward speed and D is usually defined as the chord length of the wing, μ is the viscosity of air. The Reynolds number and speed of operation are much lower than that for conventional aviation. The speeds are on the order of 1 m/s and given the air viscosity is 1.98 x 10^{-5} Kg/m-s, the Reynolds number of operation of MAV flight is about 2000-20000 [3]. In this regime the performance of conventional airfoils drops dramatically because of the laminar separation bubbles (Figure 1.2 C) that lead to lower lift and higher drag coefficients. Figure 1.2 B shows the lift-drag-polar associated with the low Reynolds number flow of a conventional airfoil. As seen in Figure 1.2 B, the polar drag is higher and heavily distorted. This presents a further challenge of design of airfoils at such low Reynolds numbers for conventional

fixed wing airplanes. This problem can be partly offset by not using fixed wings. Nature has determined the solution in the form of flapping wings. As the scale gets smaller, insect-like flapping wings provide a more attractive solution to the flight. These features include separated flow in the form of shed vortices that work to enhance lift, thrust and efficiency [3]. The efforts to imitate the flapping of insects have not resulted in successful prolonged flight due to the lack of sufficiently long lasting and high energy density power sources (Figure 1.4), and the complexity of the motion to be replicated (Figure 1.5).

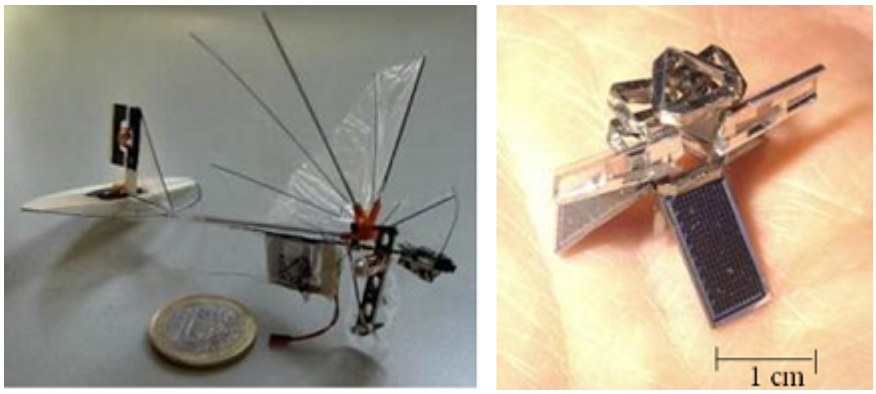

Figure 1.1: Typical size of MAV's. (Left) Delfly MAV with wing span of 10 cm. and (Right) Harvard Microrobotic Fly with a wing span of 3 cm.

1.1.1 Energy and Power requirements for a MAV

Power needed for a MAV can be divided into two parts [1]. The induced power that is needed to impart momentum to the fluid around in order to stay aloft and the profile power that is needed to overcome skin friction and drag. Induced power is highest during hovering, since in forward flight the relative flow available to the wings provides extra lift. So design for hovering should suffice for forward flight power requirement as well. Induced power (in mW/g)

	Mass	Flight time	% Battery mass
Delfly[6]	3 grams	15 min	33
Locust[7]	2 grams	3 hours	50

Table 1.1: Comparison of Flight times of Locust vs. Delfly

in all mechanical MAV can be estimated by the formula [1]

$$P_{ind} = 14.0nR\left(\frac{\Phi C_L}{AR}\right)^{\frac{1}{2}} \tag{1.2}$$

$$P_{pro} = 18.2nR\left(\frac{C_{D,pro}}{C_L}\right) \tag{1.3}$$

where n is the flapping frequency in Hz, R is the length of the wing in centimeters, Φ is the angular displacement in radians (which for most insects is $2\pi/3$ radians), AR is the dimensionless wing aspect ratio (typically 0.5-0.7), and C_L and $C_{D,pro}$ are the dimensionless lift and profile drag coefficients respectively. Some power would also be needed to flap the wings, but in this case it can be neglected assuming that sufficient elastic energy can be stored so as to flap with negligible power [1]. Power required by the actuators that navigate is negligible with respect to locomotion power, and it is also used intermittently during maneuvering [1]. For R = 5 cm, n= 30 Hz, AR =0.7 and $\theta = 2\pi/3$, the total power can be estimated to be 50 mW/g (Figure 1.3). This is a lower bound for the power needed as the flight will also require wing motion energy [1]. The metabolic rates of insects are infact in this range [4]. Table 1.2 shows the metabolic rates of various insects. As can be seen the metabolic rates are in the range of power required for flight taking efficiency into account [5].

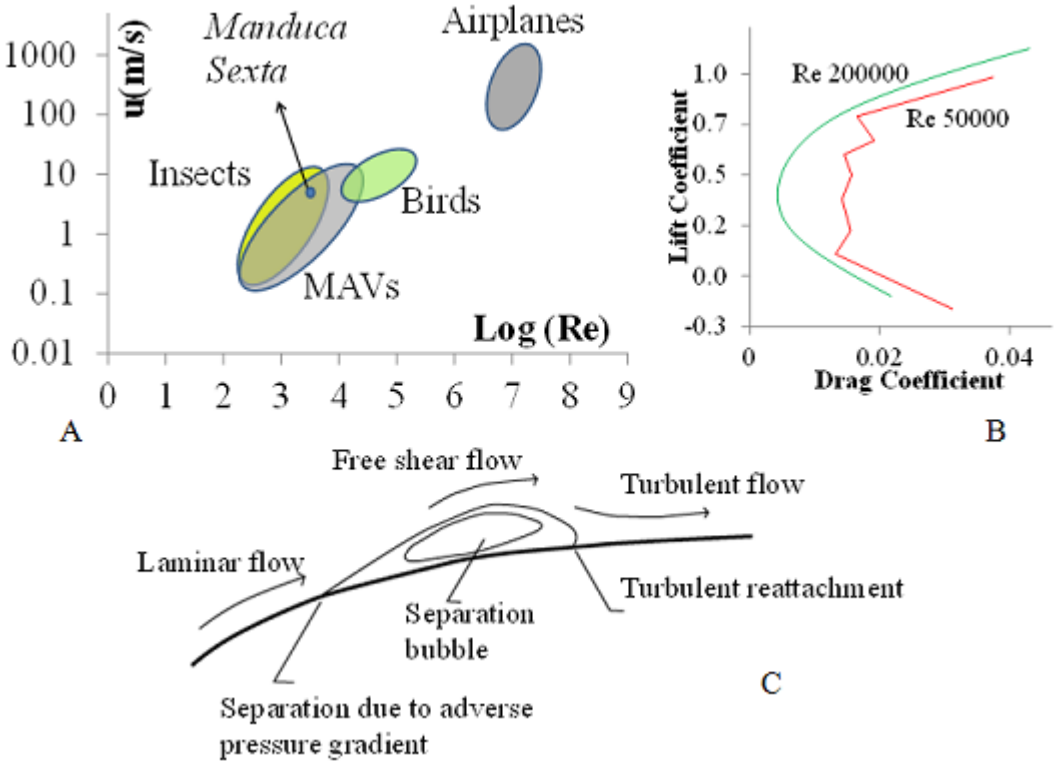

Figure 1.2: Scale of operation of MAVs and associated problems. Top left: (A) Plot of Reynolds number of various flying objects/ animals. Top right: (B) Distorted Lift-drag-polar of low Reynolds number flight. Bottom: (C) Separation bubbles at low Re

Species	Specific Metabolic rate (mW/g)
Manduca Sexta	237.0 ± 10.4
Manduca qunquimaculata	268.4 ± 16.4
Hyles lineata	346.3 ± 18.0
Hyles euphorbia	302.2 ± 12.0
Deilephila elepenor	327.9 ± 13.1

Table 1.2: Experimentally observed Metabolic rates in various insects

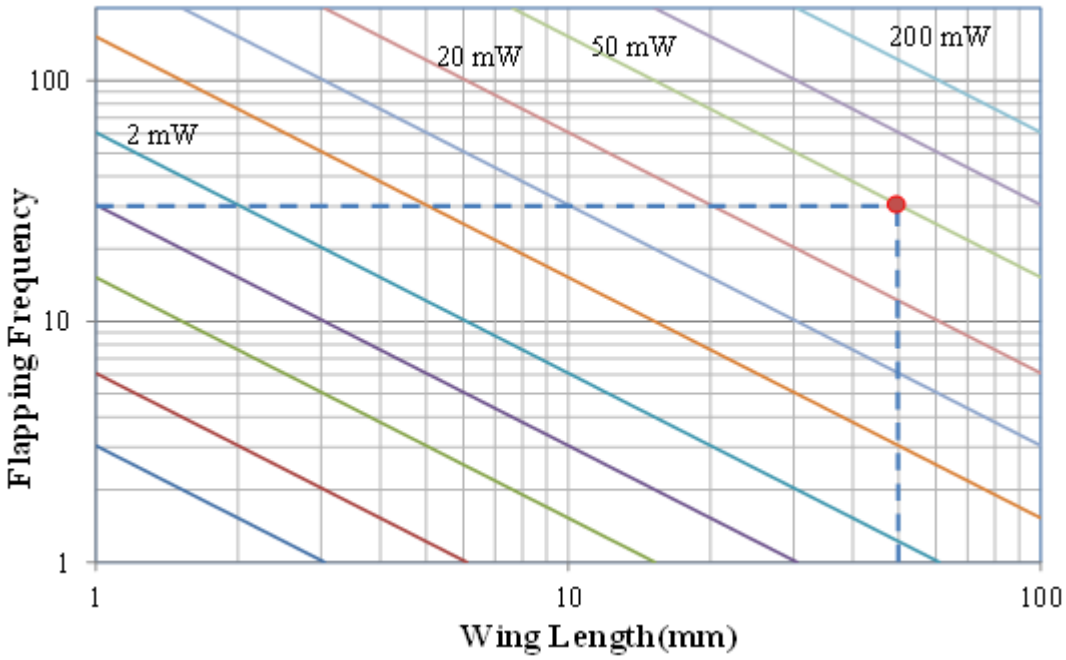

Figure 1.3: Power required for flight as a function of wing length and frequency for a micro air vehicle calculated using Equation (2) and Equation (3). The point marked corresponds to a wing length of 5 cm and a frequency of 30 Hz.

1.1.2 Energy Density and other limitations of Mechanical MAVs

Figure 1.4 shows the energy density of various power sources. As can be seen, the energy density (MJ/Kg) of fat molecules and carbohydrates are far higher than that of conventional batteries. The power density requirement for typical MAV shown in Figure 1.3 is on the order of 50 mW/g. A battery density of 3 kJ/g (Lithium batteries), would result in a flight time of 15 minutes assuming 100% efficiency of battery to mechanical conversion. Typically the electromechanical conversion efficiency for low power motors (<1 HP) is between 30-60% [8]. The energy density of fat and sugars, fuel which is used in insects, is one

order of magnitude higher energy density than that of traditional Lithium batteries. Furthermore, the efficiency of fat/sugar to mechanical motion via muscle is estimated to be 10% [9]. For an insect weighing 2-g, and the abdomen storing 50% of body weight in fat would give 126 minutes of flight time. Of course insects also refuel by drinking carbohydrates from flowers etc. Hence, the flight time of mechanical air vehicles is far lower than that of insects. For example, the

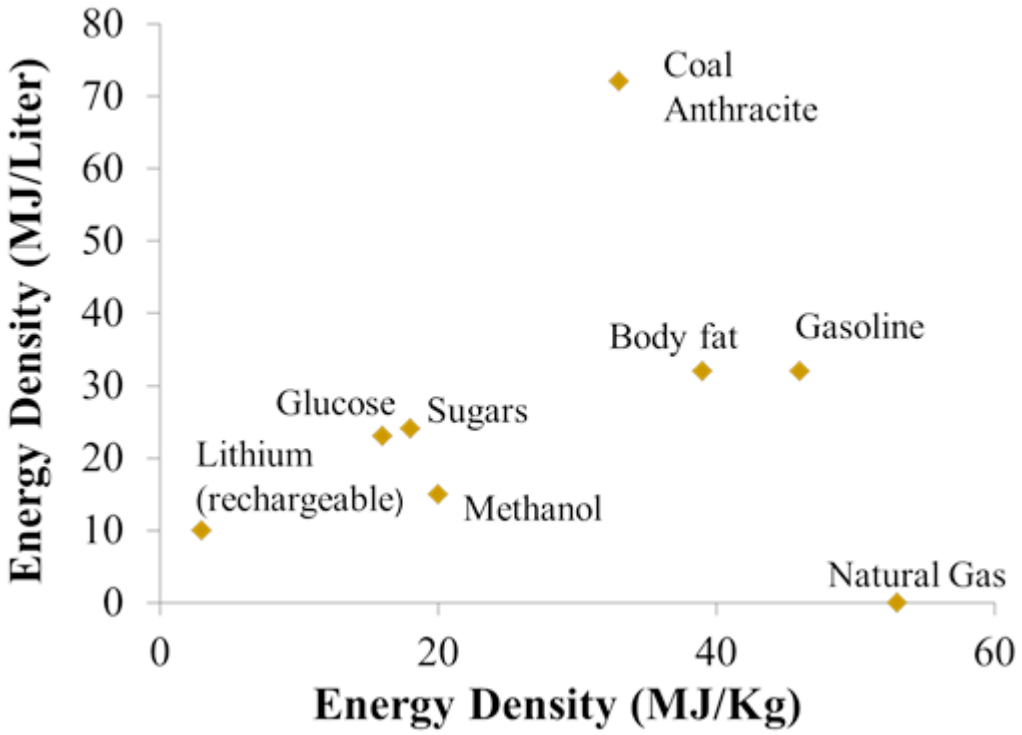

Figure 1.4: Comparison of energy density of various power sources. As can be seen the energy density of body fat and sugars far exceed that of conventional Lithium batteries enabling higher flight times for insects that that of similar scale MAVs

Delfly, which to the author's knowledge is one of the most successful flapping wing MAV, has continuous flight time of only about 15 minutes [6], while some locusts can have continuous flight times as high as three hours [7]. Another difficulty is the replication of the complex wing movements of insects in man

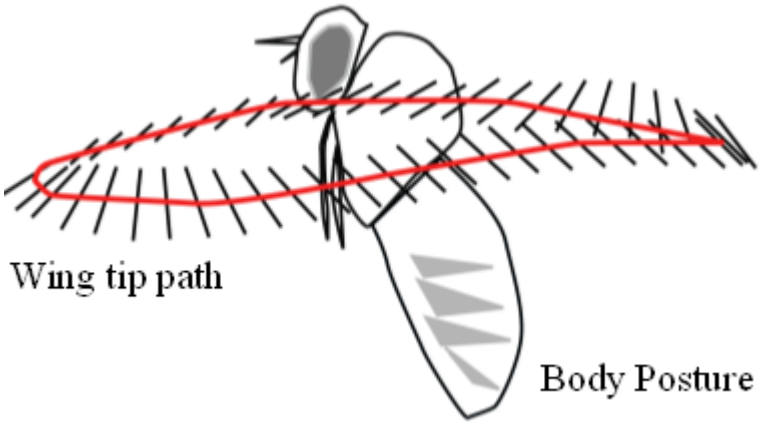

Figure 1.5: Typical wing-tip path and the wing orientation in hovering flight. As seen the wing rotates between half-strokes to strike the fluid at the correct angle.

made MAVs. Even if the flapping motion were successfully replicated, the next step is to control and ensure stability in the presence of external disturbances as flapping flight is inherently unstable.

So far no exact analysis of flapping flight has been carried out [10]. So controlling insects involves placing and operating several sensors and incorporating sophisticated control equipment. These sensors and actuators might consume additional energy and add weight, further increasing the power required for flight. These factors might offset some of the advantages gained by artificial flapping flight [2].

1.1.3 Motivation

Given the above limitations of a Mechanical MAV compared to an insect, one can envision using an insect directly as a Micro-Air-Vehicle by interfacing it with an electronic interface backpack control the flight of the insect resulting

in an Insect-Powered-Micro-Air-Vehicle (IPMAV). There are several factors that would provide strong reasons for insects to be used as IPMAVs which are described as follows:

1. The number of insect species far outnumbers that of the vertebrate species on land enabling one to choose an insect from local environment [11].
2. Insects can survive in adverse environments. For example insects can survive extremely dry environments, partly due to their biology that conserves water loss [12]. This is achieved by first storing sufficient water with Glycogen while in the larval stages, and minimizing water loss through the impermeable exoskeleton.
3. Insects provide stealth by meshing easily with local environment [13].
4. Insects have superior flight dynamics that have evolved over 300 million years of optimization [14]. Research has showed that insects rely primarily on unsteady aerodynamic forces such as delayed stall, rotational circulation, and wake capture to generate extra lift that helps to keep themselves airborne as well as reduce power requirement for flight [15]. This is in contrast to fixed wing mechanical airplanes that primarily rely on steady state aerodynamic forces to generate lift.

Several factors relating to the biology of the insect enable interfacing with a backpack like device to control the insect.

1. **Development:** Experiments by Wigglesworth on the role of brain and hormones in the development and metamorphosis of insects have revealed that the metamorphosis and development can go largely unhindered even

in the presence of external objects such as capillary tubes inserted in to the brain [16]. Thus one could include foreign objects as an interface to the organism in order to provide some functions.

2. **Payload Capacity:** Telemetry experiments on insects to record muscle potentials during free flight reported payload capacities in excess of 20% of the body weight [17]. Insects also go through metamorphosis during their developmental cycle that enables manipulation of adult size. Larvae can be made bigger by providing hormones, thus delaying pupation and leading to larger adults [16].

3. **Navigation:** Unlike land organisms, air-flying insects have low inertia making them easier to navigate or turn once they are airborne. Insects can also use their vision to avoid obstacles etc, and can be used for collision free flight which otherwise requires high levels of computational complexity, if the user has to navigate without actually being aware of the environment in which the MAV is flying [18]. So, if properly controlled, one can use insects as MAVs with minimal flight control capability in areas that humans cannot otherwise access without seriously jeopardizing their own safety.

4. **MEMS Technology:** Advances in Micro Electro Mechanical Systems (MEMS) fabrication techniques have enabled development of MEMS devices that can interface biological tissue. Examples of such devices include cardiac and neural probes [19], brain machine interfaces and targeted drug delivery devices [20] that can be embedded into body tissue. Such devices can be used to provide MEMS based interface to the insect anatomy.

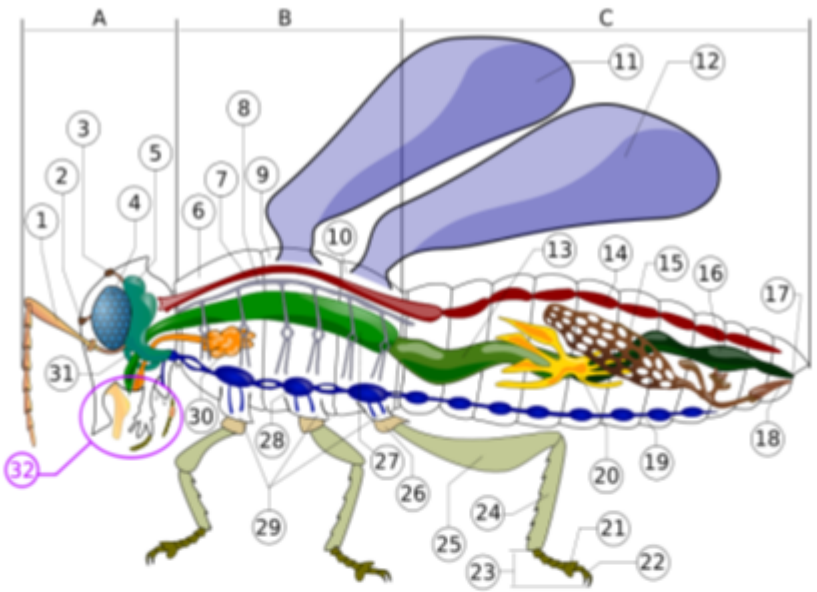

A - Head B- Thorax C- Abdomen

1. antenna
2. ocelli (lower)
3. ocelli (upper)
4. compound eye
5. brain (cerebral ganglia)
6. prothorax
7. dorsal blood vessel
8. tracheal tubes (trunk with spiracle)
9. mesothorax
10. metathorax
11. forewing
12. hindwing
13. mid-gut (stomach)
14. dorsal tube (Heart)
15. ovary
16. hind-gut (intestine, rectum & anus)
17. anus
18. oviduct
19. nerve chord (abdominal ganglia)
20. Malpighian tubes
21. tarsal pads
22. claws
23. tarsus
24. tibia
25. femur
26. trochanter
27. fore-gut (crop, gizzard)
28. thoracic ganglion
29. coxa
30. salivary gland
31. subesophageal ganglion
32. mouthparts

Figure 1.6: Schematic diagram of the insect showing the three main regions and various bodyparts

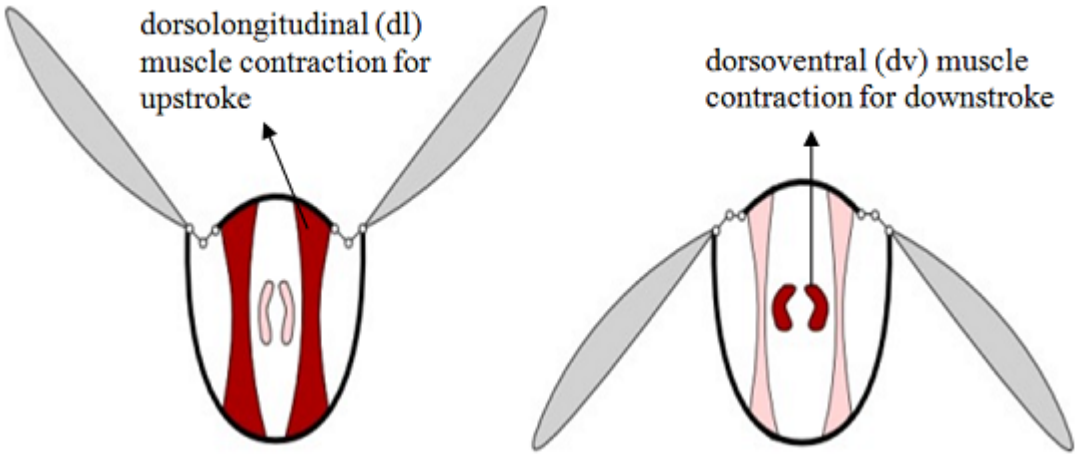

Figure 1.7: Schematic showing the thoracic compartment of an insect with indirect wing muscles and the contraction of muscles to actuate the wings. Contraction of *dv* muscles produces upstroke and contraction of *dl* muscles produces downstroke

1.2 Insect Anatomy and Life Cycle

Below we describe the basic anatomical features and various developmental aspects of the insect starting from the egg to the adult with emphasis on features that provide a favorable setting toward the realization of an Insect Powered MAV.

1.2.1 Anatomy and Morphology

Figure 1.6 shows the anatomy of a typical insect. The three main parts of the body that are easily discernable are [21]:

1. **Head:** The head capsule is a compartment that houses the brain, a mouth opening, mouthparts used for ingestion of food, and major sense organs (including antennae, compound eyes, and ocelli).

2. **Thorax:** The second (middle) tagma of an insect's body is called the thorax. This region is exclusively adapted for locomotion – it contains three pairs of walking legs and in many adult insects, one or two pairs of wings. Structurally, the thorax is composed of three body segments: prothorax, mesothorax, and metathorax. These segments are joined together rigidly to form a box that houses the musculature for the legs and wings. While the exact details of various muscles in the thorax can be quite complex, a simple model representing the muscles in the thorax in *Manduca Sexta* is shown in Figure 1.7. There is symmetry in the arrangement of muscles of which two groups of muscles are prominent. The dorso-longitudinal (*dl*) muscle, which is responsible for downstroke and the dorso-ventral (*dv*) muscle, which is responsible for upstroke. Symmetrical arrangement and the separation of the control of downstroke and upstroke might facilitate control of individual wing movements.
3. **Abdomen:** An insect's abdomen is the third functional region (tagma) of its body; the abdomen is located behind the thorax. Each segment of the abdomen consists of a dorsal sclerite, the tergum, and a ventral sclerite, the sternum, joined to one another laterally by a pleural membrane. The front margins of each segment often "telescope" inside the sclerites of the preceding segment, allowing the abdomen to expand and contract in response to the actions of skeletal muscles. This helps the insects pump fluid to inflate the wings after emergence. These actions also facilitate the abdomen to act as a rudder helping to steer insects when in flight.

We chose *Manduca Sexta* as our experimental subject since we believe it is quite suited to the research for several reasons. The tobacco hornworm *Manduca Sexta* is a popular experimental animal in biology that is used in the study

of a diverse array of biological problems ranging in topic from basic ecology and growth, to neurobiology, muscle physiology and the biochemistry of camouflage. *Manduca Sexta* is easy and inexpensive to grow in the lab environment, is relatively large, has simple body systems, has a complete (and relatively fast) life cycle, and is free of the ethical issues surrounding more complex or endangered organisms. *Manduca Sexta* is also a powerful flyer [22]. Thus all the existing knowledge of biology relating to *Manduca Sexta* can be readily taken from literature, making it a promising subject for studies that that involve trying to use it to carry a "backpack-like" device that can manipulate its behavior and enable its use as MAV [23].

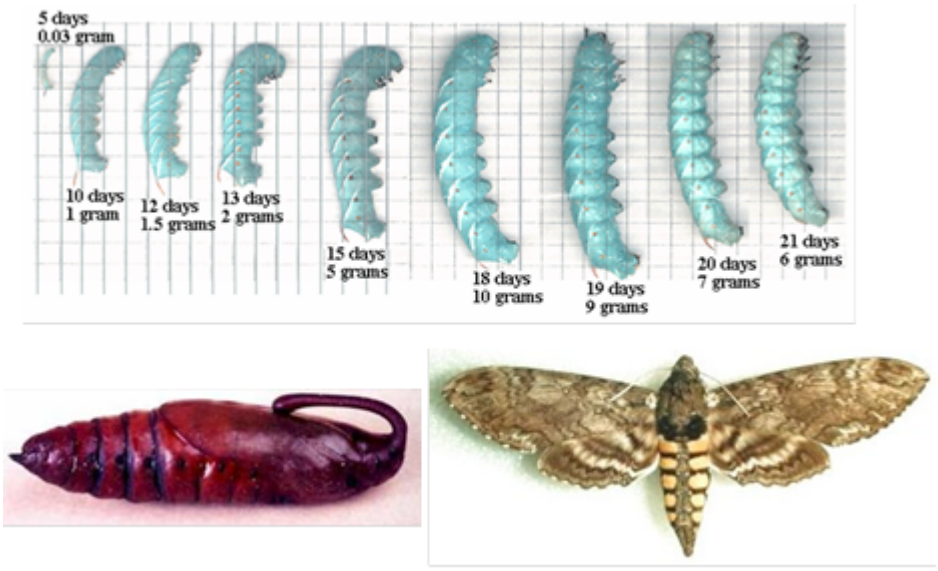

Figure 1.8: The life cycle of *Manduca Sexta* showing the development from larvae to the adult

1.2.2 Development and Metamorphosis of *Manduca Sexta*

Most of the major insect orders have a typical life cycle which starts with an egg, which hatches into a larva which feeds, molts and grows larger, pupates, then emerges as an adult insect that looks very different from the larva. In *Manduca Sexta* (Figure 1.8) the development starts with an egg. Larvae hatch from their tiny, pale green eggs three to five days after the eggs are laid. These newborn or first instar larvae are only a few millimeters long and very pale green. As the larvae get older and larger they become bright green with seven pairs of lateral white stripes bordered with black. The 70 mm long larva climbs down from its host plant and begins a period of vigorous walking or wandering that typically lasts for about five days. During this stage, gut contents are voided, body moisture is lost, and a dark bluish line or dorsal heart becomes visible along the larva's back. At this point, the larvae bury themselves about 9 - 15 inches deep underground, in loose soil or leaf litter. After a few days, the buried larva molts a final time to form a light green pupa. Over the first few hours, biochemical reactions cause the pale green skin or cuticle of the new pupa to harden and turn dark brown. During the three-week pupation period, tissues are reorganized to form the structures of the adult *Manduca Sexta*. This stage of metamorphosis is very attractive phase for integrating the insect with foreign probes or devices since it provides a stage where there is very little tissue and hardly any well-formed organs inside the body. Inserting a foreign object does minimal or even negligible damage to any vital organs. Thus it enables one to insert components during the developmental stages with minimal tissue or organ damage and obtain an adult insect with the components that are fully embedded with proper tissue development around the inserts providing a reliable bioelectrical interface.

1.2.3 Senses and Communication

Many insects possess very sensitive and specialized organs of perception. Senses can be divided into olfactory, auditory and visual. Distinct stereotypical responses to sensory stimulus can help navigate the moth by using its instincts to say smell on one side and sound on one side leading to locomotion guided by senses. *Manduca Sexta* has been extensively studied with respect to its senses especially olfactory response.

1. **Vision:** With respect to vision, *Manduca Sexta* can perceive infrared wavelengths, and detect polarized light [24]. Many insects also have an optomotor response where the behavior is influenced at every step, by the stimuli to which eyes are subjected to [25].
2. **Olfactory:** *Manduca Sexta* is sexually dimorphic with respect to the olfactory system. Male antennae are enlarged and contain elongated sensilla (sensory organules) not present in females [26]. The pheromone elicits a male response by stimulating male specific receptor cells on a large number of these sensilla, which are located on the antennal flagellum. The antennae of male moths can detect the pheromones of female moths over distances of many kilometres.
3. **Auditory:** Being nocturnal moths, *Manduca Sexta* can perceive the ultrasonic emissions of bats, a mechanism which helps them avoid predation. There is also evidence that Noctuid moths can locate a sound source in a three dimensional space by analysis of the changing intensity of the sound in the two ears during the wing-beat cycle [27]

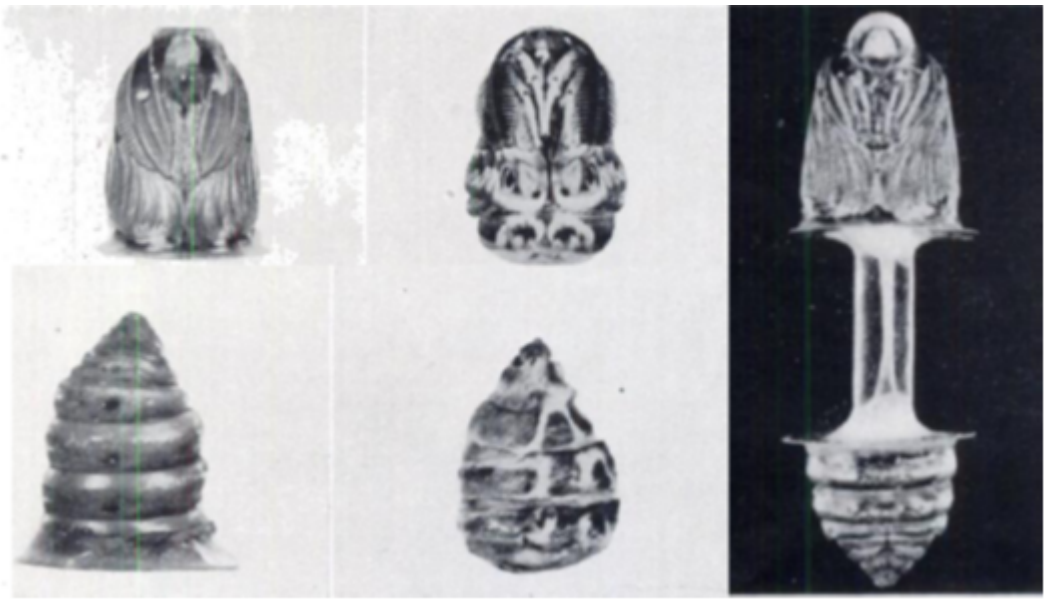

Figure 1.9: Experiment showing the dissection of pupae and their subsequent development. Figure also shows the connecting tissue forming through a tube.

1.3 Early Metamorphosis Insertion Technology (EMIT)

The success of the IPMAV depends on how well the device or backpack can be integrated into the insect. Here we describe some of the risks of integrating a backpack into the insect and the possible ways to overcome those risks.

1.3.1 Challenges involved in integrating insects with control devices

One of the primary risks involve in integrating a device into the insect at the adult stage include the insect failing to assimilate the probe and possibly suffering from a wound and the risk that the ensuing complications might result in

death of the insect. In addition a reliable bioelectrical interface is also needed. In the absence of such an interface the backpack may not fully perform the desired function. One of the ways to solve the above problems is to insert the device during early stages of metamorphosis. As has been described, during metamorphosis most of the tissue is reformed and since in the early stages of metamorphosis there is no tissue formed, all the insertions can be done with minimal damage to the tissues. The injury would also heal as the tissue is developing and results in a reliable bioelectrical interface to the insect. One of the challenges involved in realizing an Insect Powered Micro Air Vehicle is that of integration of the device with the insect. Several experiments were performed that showed insects can survive insertion of foreign objects during the pupal stages without significantly delaying or inhibiting their ability to develop into full grown adults. Insertions done at different pupal stages produced adults that had components embedded in them. Earlier work along these lines included work by Wigglesworth intended to study the causative mechanisms behind metamorphosis in insects. Figure 1.9 shows a sample experiment in which a pupae was cut into two and when the two halves are disconnected, the bottom half develops only when the organ secreting juvenile hormone (JH) is transferred to an adult while the one without remains a pupae. But when they are connected with a tube, and JH gland is implanted in the lower half, one can see nerves growing in through the tube. These experiments apart from uncovering the mechanisms behind metamorphosis also indicated that insects can develop into full grown adults despite significant intrusion into their bodies [28].

1. **Thoracic Inserts:** Silicon (Figure 1.10) and polyimide probes were inserted into the thoracic muscles of the insect during early stages of metamorphosis (within 5 days of pupation). The silicon microprobe platform (500

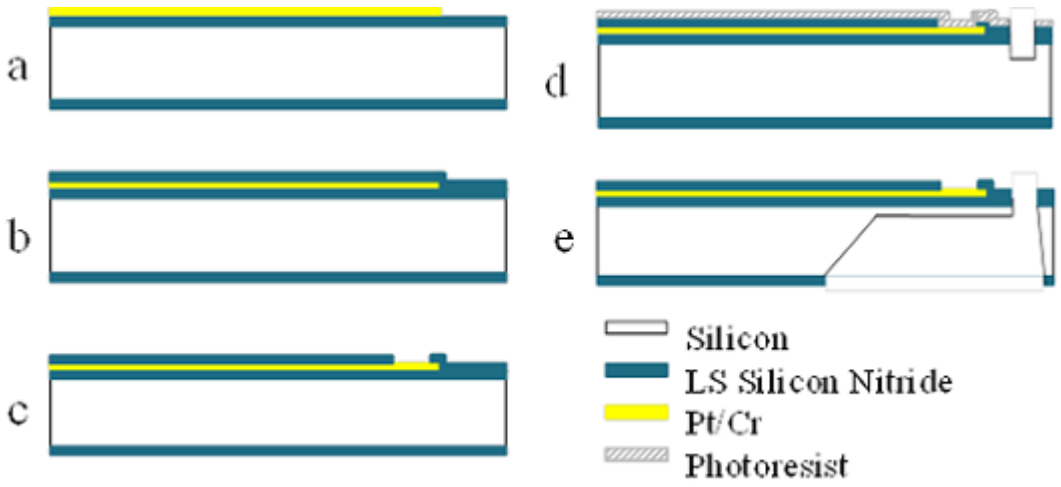

Figure 1.10: Fabrication of silicon based probes for insertion into the thorax of *Manduca Sexta*.

μm thick) consists of 2 tips (each 200 μm wide, 200 μm thick and 5 mm long) separated by a distance of 5 mm, which is the approximate distance between the right and left flight muscles of the moth (Figure 1.11). Platinum (electrode metal) was evaporated and patterned on a 4" silicon wafer with a layer of 900 nm LPCVD nitride. PECVD nitride was deposited on the metal and patterned to provide passivation. The metal lines running along the length of the probe tip, that actuate the muscle cells were only exposed close to the end of the tip (100×100 μm^2) for muscle specific excitation (Figure 1.11). The desired probe tip thickness was achieved by deep reactive ion etching (DRIE). Backside-only KOH etching (with LPCVD nitride mask) was done to release the device [29]. Figure 1.11 shows a pupa with the inserted probe. To place the probe in the thorax, firstly the pupae was placed on ice, in order to reduce the internal hemolymph pressure. This would prevent the oozing of hemolymph out of the pupa. Then two incisions were made with the same separation as that of the probes using a hypodermic needle since the stiffness of the probes was not enough

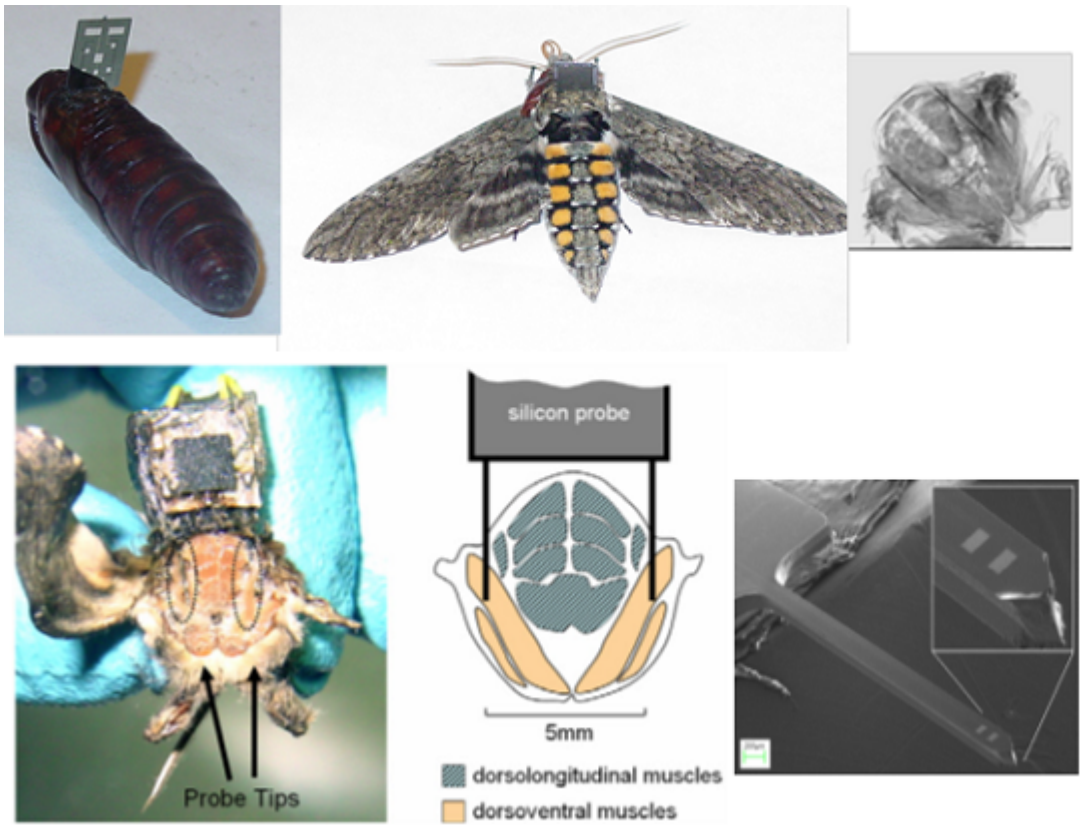

Figure 1.11: (Clockwise from top): 1. A pupa with the probe inserted. 2. An adult that emerged out of the pupae with the insert inside the thorax. 3. An X-ray image of the thorax with probes in the dorso-ventral (*dv*) muscles showing normal development of the muscles in the thorax. 4. An SEM image of the probe tips showing the metal pads for muscle stimulation. 5. A schematic of the thoracic muscles and the regions targeted by the probe. 6. Cut section of the thorax showing the probe and the target muscles.

to penetrate the cuticle. The probes were rinsed in alcohol and insertions were made into the mesothorax. The probe is shown in the Figure 1.11. The probe was inserted approximately 0.5 cm inside the surface of the cuticle straight inside. Once the probe was inserted, the opening was quickly sealed with molten wax in order to prevent loss of blood. Near 100% emergence rates were obtained.

Dissections of the thorax were performed to observe the successful insertion of the probes near the target muscle groups (Figure 1.11). Muscle growth around the probe tips indicates successful adaptation by the moth body. In order to further ensure that the development of the internal organs and muscles was similar to that of a normal moth Micro-CT scans were performed. The images showed normal tissue growth inside the thorax and around the inserted probes. Although the thorax contains many muscles, bulk of the thorax constitutes only of the dorso-ventral (*dv*) and the dorso-longitudinal (*dl*) muscles. These muscles also have distinct left and right divisions that enable independent actuation. These probes were designed to reach the dorso-ventral (*dv*) muscles and can be used for targeted muscle actuation.

2. **Abdominal Inserts:** Polyimide capillaries (outer diameter: 220 μm, inner diameter: 150 μm) and Ti wires (100 μm) were inserted into the abdomen and the thorax of the insect so as to reach the muscles or the stomach. Capillaries can serve as microfluidic interfaces for food (such as sugar) into the stomach and Titanium (Ti) wires could be used to excite muscles by reaching into the thoracic cavity. After chilling the pupa on ice to prevent heamolymph leakage, a hole was punctured using a hypodermic needle and a capillary or Ti wire was inserted to reach the abdomen or the thoracic muscles. The opening was then sealed using molten wax. Similar to the case of thoracic insertions, Micro CT was performed on the insect to look for the development of the internal organs in the presence of capillaries (Figure 1.12). The imaging revealed that the internal organs developed properly. Histology was also performed to investigate the assimilation of the capillary into the body by looking for scar tissue around

the inserts. Figure 1.12 shows TEM images of the capillary section along with tissue around it. High magnification images show cells around the capillary intact and organelles inside the cells can be seen at an even higher magnification indicating that the cells were healthy. While the success rate of emergence was nearly 100%, some of the adults had malformed wings due to insufficient pressure while inflating the wings. About 50% success rate was obtained with moths with completely formed wings.

3. **Abdominal Segment Removal:** Some of the abdominal segments can be removed to enhance the payload capacity of the moth, by having other components instead of the abdominal segments. Although such experiments were done earlier in 1942 they were repeated now. During early pupal stage the last 2-3 abdominal segments were severed and the insect was sealed using a cover slip and dental wax. Figure 1.13 shows a moth emerged with its wings fully inflated and with two of its final abdominal segments removed. The rear is completely sealed and there is no leakage of fluids out of the insect.

1.4 Conclusion

The results presented in this chapter provide compelling reasons why insects would be well suited to the role of autonomous flying machines. The resulting IPMAV would have longer flight times as a consequence of higher energy density of bio-fuel and superior flight capability compared to any existing mechanical flying machine at comparable size, both in aerodynamic performance and flight actuation machinery. The aim of this study was to employ insects, partic-

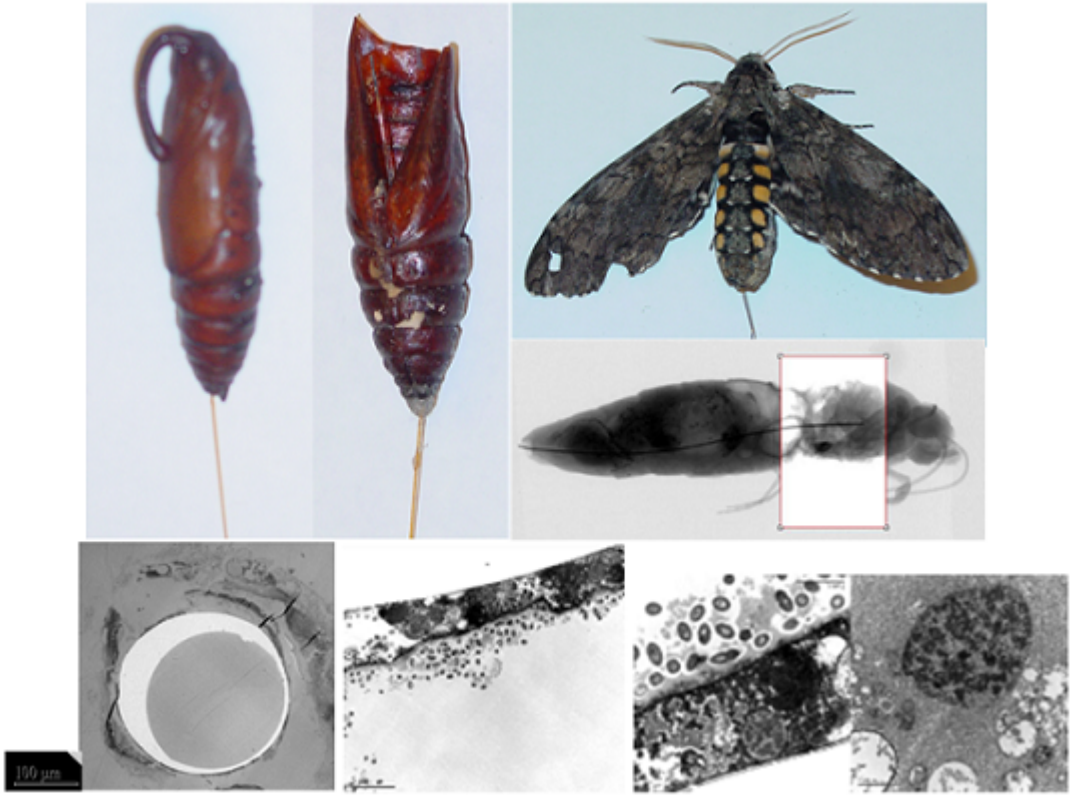

Figure 1.12: Above: Polyimide capillary inserted from behind through the abdomen into the thorax and emerged adult and its Micro CT image. Below: Histology showing the formation of normal cells around the capillary tube.

Figure 1.13: Pupa with the last few abdominal segments removed and insect that emerged out of its shell.

ularly moths, themselves as a platform to realize hybrid systems with intimate electromechanical interface to the anatomy. We have demonstrated the use of EMIT to insert microsystems in early pupae stages to obtain reliable interfaces specifically a silicon based platform was designed with respect to the position of the muscle bundles, and was inserted into the thorax within seven days of pupation. In addition a capillary based interface to easily manipulate the adults was successfully formed in the insect by placing a polyimide-capillary through the pupae. The successful emergence of the pupae proves that a backpack like device could be integrated very well with insects and can be potentially used for flight control.

CHAPTER 2

FLIGHT CONTROL OF BALLOON ENABLED INSECT FLIGHT

2.1 Introduction

Achieving control over biological locomotion has been a topic of attention of since early 20th Century [30]. Most of the earlier work centers on the idea of "Conditioning" organisms, which refers to the process of inducing a reflex or a behavioral response by providing some form of a neutral stimulus along with an unconditional stimulus. A classic example of this is Pavlov's experience with dogs. Pavlov noticed that, rather than simply salivating in the presence of meat powder (an innate response to food that he called the unconditioned response), the dogs began to salivate in the presence of the lab technician who normally fed them. While most of the work has been centered on understanding the behavior of organisms, there are two efforts that have aimed at achieving control over living organisms so as to use it as a substitute for a mechanical robot. Recent work in this area includes that of Talwar et al. [31] who realized a guided rat. The approach involved is that of a conditioning phase where the rat receives training to move left or right depending on the stimulus that is provided to the brain. While this effort and earlier efforts have been by biologists, recent advances in micro and nano technology have brought to the attention of engineers the fact that mechanical systems suffer from serious limitations in terms of force generation and energy density at the small scale. For a wide variety of applications it is believed that the mechanical systems capable of providing sufficient force within such space constraints for practical applications will most likely remain beyond actual technological means for an extended period of time [32]. One

such application is that of micro robotics to propel drug delivery devices. Martel [32] attempted to control the movements of a swarm of MC-1 magnetotactic bacterium using external magnetic field. In this case the bacterium provides the necessary propulsive force while the external magnetic field serves to control the direction. Figure 2.1 shows the trajectories along which the rat and the swarm of bacteria are controlled.

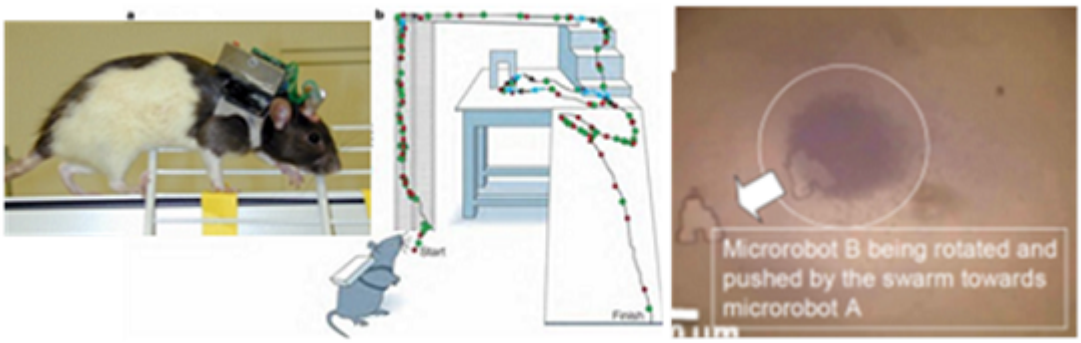

Figure 2.1: Left: A picture of the roborat and a test track showing the path followed by the guided rat. Right: A picture of the swarm of bacteria controlling a micro-device

2.1.1 Challenges involved in Insect Flight Control

Here we compare and contrast the locomotion control techniques of the previous efforts and their applicability in the case of insect flight control and present some of the primary challenges involved in insect flight control.

1. **Load Carrying Capacity:** Since the load carrying capacity of the insect is less than a gram [33, 34], the backpack that is used to control the flight should be within a gram. This presents a challenging design problem where the weight of all the components including the power source, the

receiver and the actuators has to be within a gram.

2. **Life Span and Learning Capability:** The fact that the short lifespan (typically 1-3 weeks for adults) and limited learning capability [35] precludes achieving control by conditioning or training the insects. Previous experiments on conditioning have involved mainly high level organisms with much longer life spans that have the capability to learn and develop a response to an external stimulus.

3. **Control System:** Insect has a built in control system that senses body forces and accelerations and works towards achieving stable flight. For example, the insect is known to be trying to stabilize itself when mounted on an oscillating rotary table [36] and also sense visual environment around it and stabilize itself with according to the visual input. Thus applying a torque to change the orientation of the insect would immediately trigger the feedback mechanism to restore the orientation.

2.2 Potential Strategies for Flight Control

Here we present the various strategies for flight control that can potentially be used for navigating an insect powered MAV. Figure 2.2 shows the control structure of the insect. It starts with the various sensory organs (eyes, smell, sound and wind) taking input and providing signals to the brain. The brain then processes the signals and provides stimulus to the muscles through nerves. The muscles contracts based on the neural signals provided, and actuate the wings which move to generate the necessary aerodynamic forces to fly. So as can be seen, one could envision controlling the insects by interfering with any of the

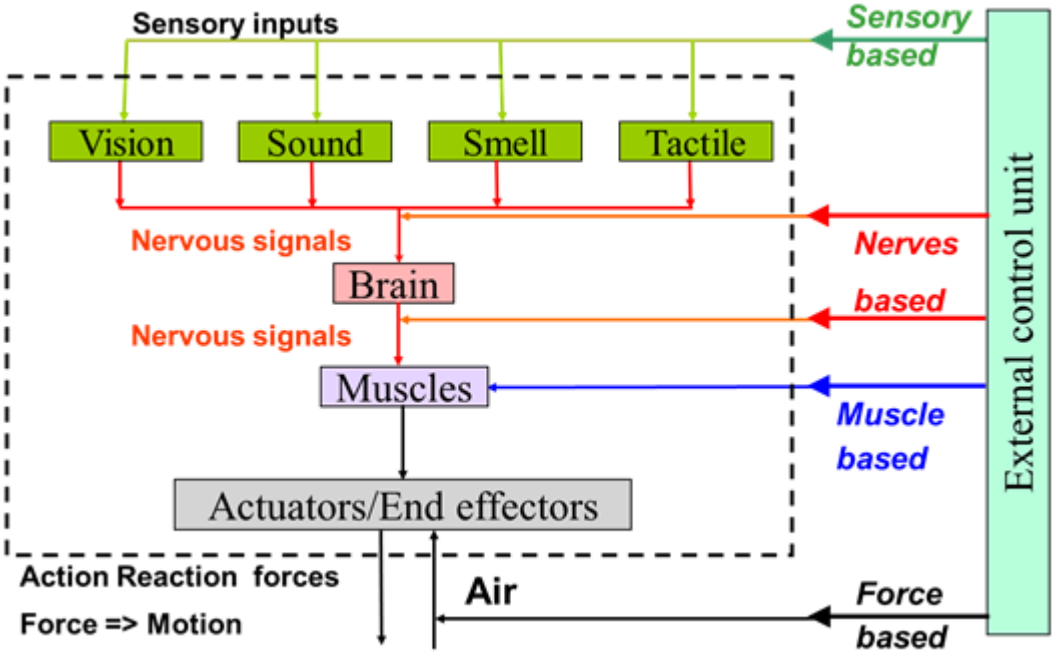

Figure 2.2: Control system of *Manduca Sexta* showing Sensory inputs followed by the brain, followed by the muscles which move the wings to realize the required aerodynamic forces.

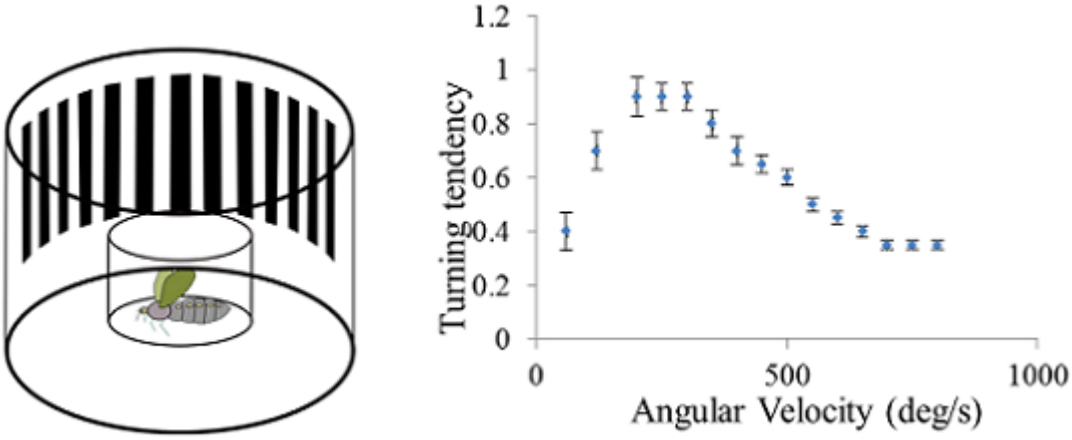

Figure 2.3: Left: The typical setup involving tracking of a visual grating and the response of the moth observed. Right: Figure shows the response of the moth as a function of the angular velocity of the grating.

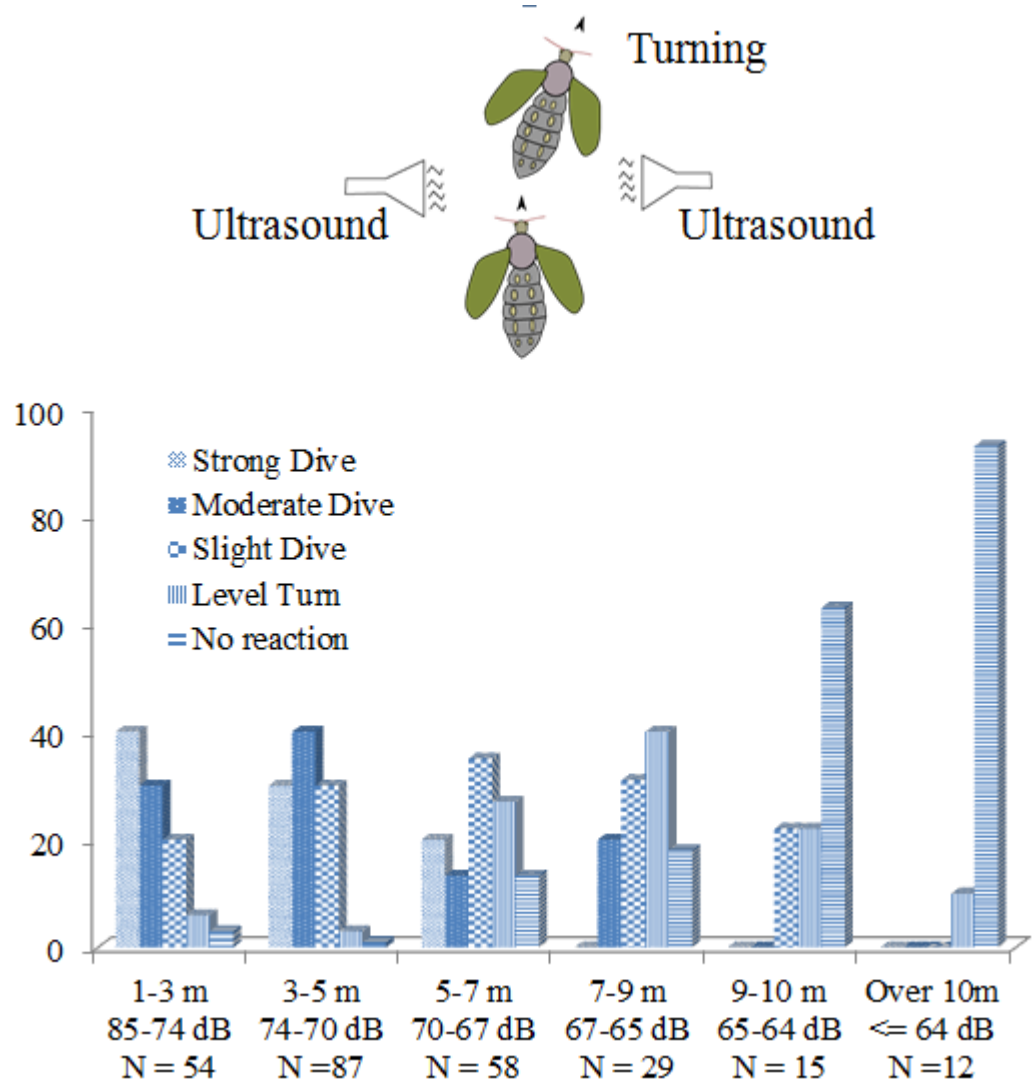

Figure 2.4: Figure showing the percent responses to varying degrees of ultrasonic intensity.

control pathways which are sensory, neuromuscular and external force based.

2.2.1 Sensory Based Control

Insects are known to have very well defined responses to various sensory inputs. Below we describe various known responses to sensory inputs.

1. **Optomotor Response:** There is strong evidence that optical stimulus is used to stabilize flight in *Manduca Sexta*. Experiments on tethered animals have indicated that visual stimuli modulate the activity of wing-steering muscles during flight [25]. A typical setup involves a visual grating surrounding the field of view of the insect as shown in the Figure 2.3. The insect responds to movement of the grating so that there is no relative rotation between the insect and the grating. Such a system could easily be visualized to be integrated to the eyes of the insect using an LED screen providing visual input to steer the insect.

2. **Auditory Response:** The ability of moths in stationary or tethered flight to react to artificial ultrasound and to the cries of bats was firmly established by Roeder [27]. Roeder studied the behavior of a natural population of free-flying but unidentified moths when they encountered various patterns and intensities of pulsed and unpulsed ultrasound generated by a loudspeaker. It was observed that when pulsed signals reached the flying moths at high intensity they induced a variety of non-directional reactions such as diving, tight turns, looping, and passively falling to the ground. Moths flying at a greater distance from the loudspeaker and presumably exposed to stimuli of lower intensity were seen to turn and fly directly away from the sound source. Figure 2.4 shows percentages of various responses by moths when subject to ultrasound of varying intensities.

3. **Olfactory Response:** Insects often orient toward olfactory signals to locate a potential food source, oviposition site, or mating partner. For many insects including moths, the detection of conspecific sex pheromones is an important stimulus for reproductive behavior. Moreover, in several species, receptivity to pheromones is highly sensitive and selective. Male

moths can orient upwind in response to a minute quantity of a species-specific blend of pheromones released by a receptive female several kilometers away [37]. However, a simple response as that of a yaw is harder to generate compared to auditory or optomotor response. Figure 2.5 shows the trajectory of a *Manduca Sexta* when subject to a pheromone source. As can be seen the trajectory is fairly complicated and does not induce a simple yaw motion in the insect.

2.2.2 Neuromuscular Control

The subject of turning control and the muscles responsible for turning have been an active area of research. Kammer [38] presented evidence that a subalar muscle is responsible for turning during flight and presented evidence of its activity during turning. *Manduca Sexta* also has power muscles which are clearly partitioned as left and right which are responsible for actuating the left and right wings, and each side has two main muscle groups as shown, which are responsible for downstroke and upstroke independently. So, either the steering muscles or the power muscles could be stimulated to control flight.

2.2.3 Mechanical Force Based Control

There are several ways of applying a mechanical force to an insect during flight.

1. **Tail Motor:** A tail motor could be used to apply a torque to the insect in mid-air. This is similar to the tail motor being used to control adverse yaw in a helicopter and also to change the direction. Mini-motors could be

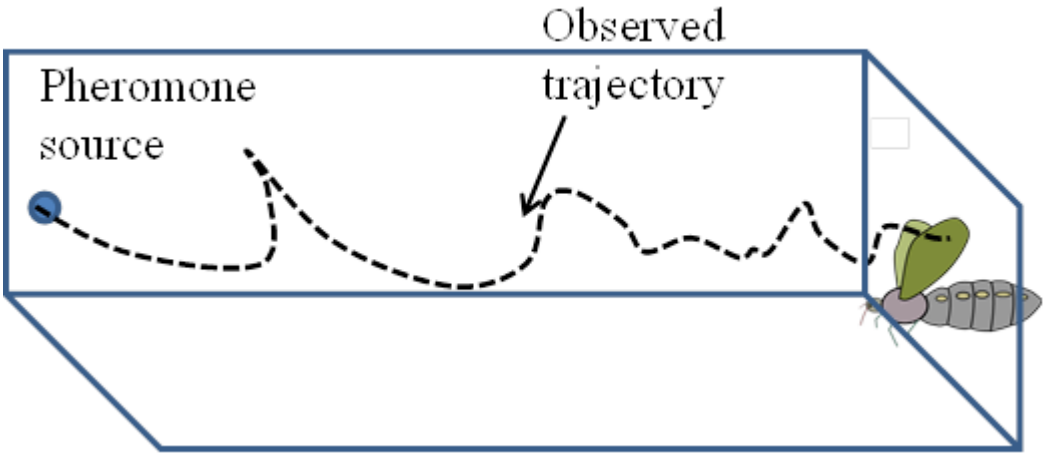

Figure 2.5: The pheromone tracking nature of the moth and the typical trajectories.

mounted on the insect to generate a transverse force (Figure 2.6). This technique can provide large amount of force and consequently a large amount of torque.

2. **Rudder:** Using a rudder can also generate a torque to turn the insect. Insect wings essentially serve to generate fluid momentum and consequently the air behind the wings has velocity of the order of 3-5 m/s. This velocity can be used to generate a force in the lateral direction using a rudder. Rudders can guide the wind momentum generated by the insect itself to control the motion. Figure 2.6 shows the principle of operation of the rudder. The flow generated by the moth behind the wings is symmetrically divided between the rudders under normal conditions. When one wishes to turn the moth in a particular direction, the rudder can be shifted left or right with the hinge actuator. The rudder acts as an airfoil redirecting the fluid behind the wings and provides transverse lift force, resulting in a moment that causes the insect to turn (Figure 2.6). Hinge actuators can be constructed to be very light weight and at the same time consume

very little power (10-20 mW), leading to long battery times [39].

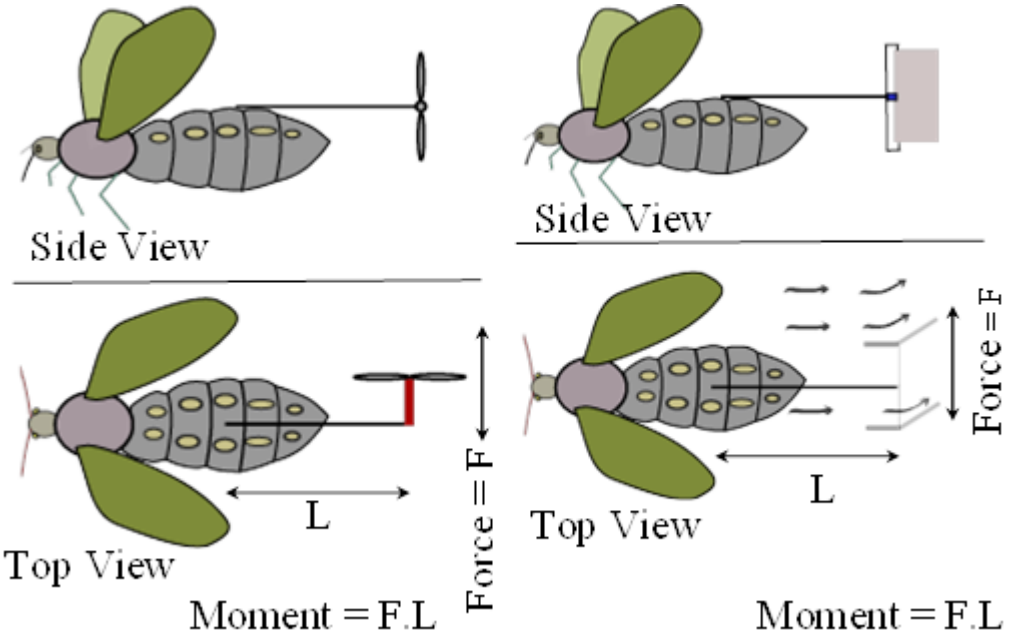

Figure 2.6: Figure shows the schematic of applying a mechanical force at the tail of the moth using a tail motor and a rudder

3. **Differential Orientation:** Another way of obtaining torque during flight of insect is that of using two insects to provide the necessary thrust force. An arrangement where two insects are aligned providing thrust forces and where they can be oriented in different directions relative to each other would serve to provide the necessary torque for turning. Figure 2.7 shows such an arrangement and the torque obtained when the insects are oriented at an angle of 2θ relative to each other. The advantage of the technique is that the torque needed for turning is partly obtained from the thrust force of the insect leading to lower power consumption and also higher force generating capability.

4. **Roll:** Roll provides a centripetal force to execute a turn. So if one could roll the insect, a component of the lift could serve as a centripetal force and

cause the insect to turn along a circular trajectory. This is similar to executing a banked turn with a component of normal reaction or lift force serving to provide the necessary centrifugal force. Figure 2.7 shows a schematic of roll based turning and the centripetal force obtained and the radius of turn.

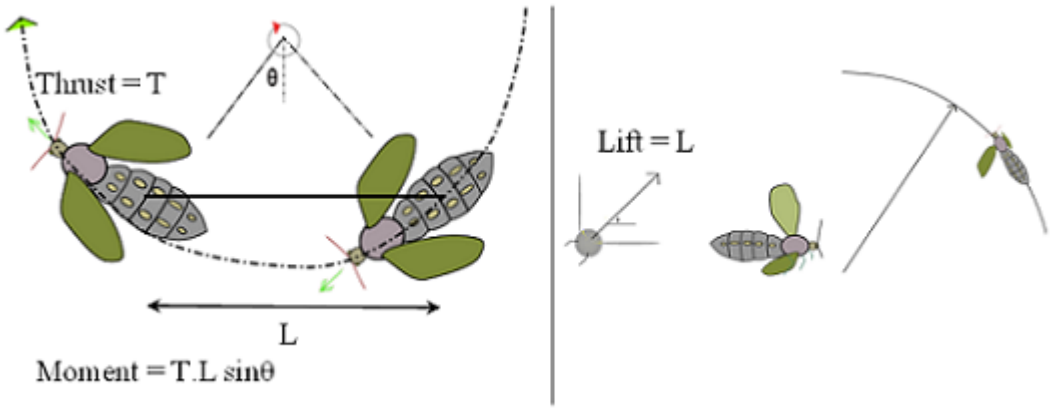

Figure 2.7: Schematic of obtaining turning behavior using differential orientation and roll based technique

2.2.4 Comparison of Various Strategies

Here we compare various above mentioned strategies with each other in terms of various metrics viz. Power requirement, weight, number of degrees of freedom controlled, whether the technique is invasive, cost, ease of assembly and experimentation and whether the technique is specific to the insect or if it can be interchangeably used with other insects (Table 2.1). As can be easily surmised, mechanical force based control has several advantages over other mentioned techniques which are listed below:

- The technique is non-invasive and hence does not deteriorate the flight

Comparison of various strategies			
Metric	Sensory	Neuromuscular	Mechanical
Power requirement	High	Low	Moderate*
Weight	High	Low	Moderate
No. of D.O.F's controlled	Low	High**	High
Strain on insect	Low	Moderate (invasive)	Very Low
Cost	High	High	Very Low
Ease of assembly	Difficult	Difficult	Simple
Insect specific	Yes	Yes	No
Insect's own control system	Doesn't interfere	Very likely interferes	interferes

*Conservative estimate. Assumes actuators are either motors or hinge actuators.
**Assumes all D.O.Fs of the insect can be controlled using neural signals.

Table 2.1: Table shows the relative merits of each of the techniques discussed in the previous sections.

capability or load carrying capacity of the insect.

- The back pack could be constructed with commercial off the shelf components. The lack of the need for custom made components greatly reduces the cost compared to other methods of navigation.
- The technique is also not insect specific as long as the insect is in a similar size category. A back pack constructed for *Manduca Sexta* might be used for another similar insect.

2.3 Mechanical Force Based Flight Control Experiments

Experiments were performed to test the feasibility of each of the above mentioned techniques of navigation. Initially tethered flight experiments were conducted to check the feasibility of each of the techniques in tethered flight. Untethered flight experiments were then performed using a balloon enabled system.

2.3.1 Tethered Flight Experiments

Attempts were made to control the orientation of the moth in tethered flight. In order to attach the insect to the tethered setup, its body temperature was first cooled to 4°C by placing it in the refrigerator for 30 minutes. This renders the insect unconscious and immobile. The insect was then attached to a basswood stick using a drop of Tackiwax on the upper part of the abdomen just below the thorax (Figure 2.8 A). In order to attach the insect along with the basswood stick to the tethered flight setup we made use of dual magnet system that prevents relative rotation between the magnets (Figure 2.8 B).

Tail Motor: The tethered flight setup included attaching the insect along with the receiver, battery and motor for remote control to a wooden shaft that was suspended from a bearing, allowing free yaw motion. A Plantraco 4-mm diameter 13-Ohm micromotor was used along with a 32-mm diameter propeller to apply an external torque. As a torque was applied, it was observed that the insect would turn in the direction of the moment but stop turning at one point. When the torque was removed, there was a small motion in the reverse direc-

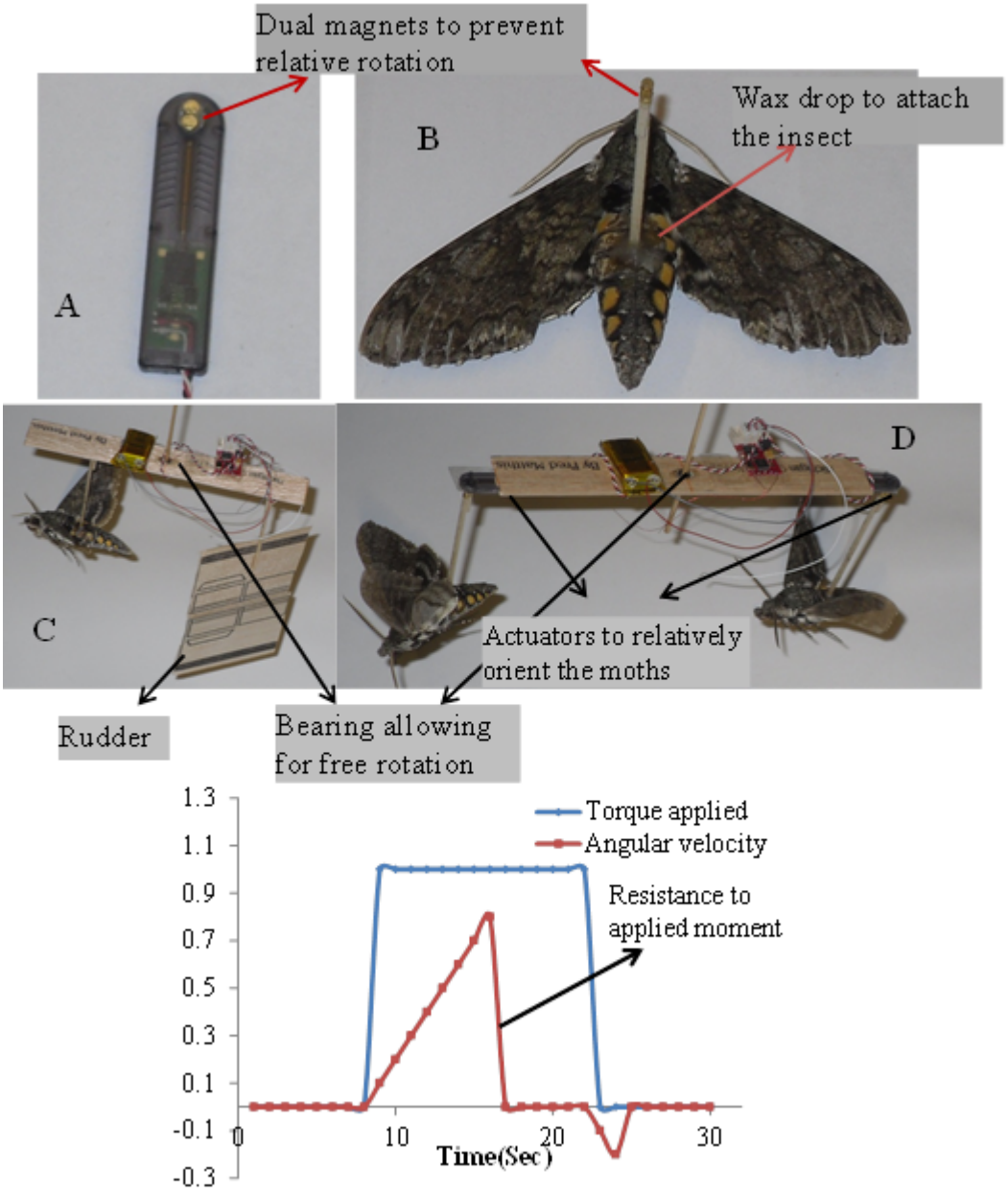

Figure 2.8: Figure shows the attachment of the insect to the back of the thorax using Tackiwax and the dual magnet system used for attachment B: The actuator used to implement the relative orientation and rudder. C: Tethered setup of Relative orientation. D: Tethered setup of Rudder based control. E: Typical response observed with an application of torque to the insect

tion, possibly due to the resisting moment. Such behavior has been previously reported and is due to the sensors in the insect that sense the rotation of the insect and provide the necessary forces to stabilize the insect [36]. Even at the loss of apparent control, this technique enables one to very effectively control the amount of moment that is being applied with motors weighing less than 0.1 gm [40]. The moment can be further amplified just by increasing the distance from the center of gravity of the moth. But the main drawback is the power consumed by the motor at the tail, which can be 100's of milliWatts for even the tiniest of motors, limiting overall mission times.

Rudder: A Plantraco MicroAct actuator was used to steer a rudder and attached to the tail of a beam, while a moth was attached to the front of the beam using adhesive bonding. The orientation of the combined system was altered in tethered flight, proving the feasibility of rudder-based navigation [41]. But similar to steering using tail motor, continuous change of direction was resisted by the moth. The hinge actuator was 0.41 gm in weight and had a coil resistance of 50 ohms, and required 1 volt resulting in an average 20 mW of power consumption [39]. The hinge actuator was placed approximately 5 cm from the tail of the insect. The rudder had an area of 25 cm^2. This type of navigation can be used immaterial of the forward velocity of the insect since there would always be fluid flow behind the wings whether the insect is hovering or in peak forward velocity flight. It is interesting to note that although magnetic hinge actuators were used to realize the motion of the rudder, they can also be realized with much lower power consumption with piezoelectric actuators [42].

Differential Orientation: A prototype of this system was built using hinge ac-

tuators and the relative orientation of the moths was adjusted [41]. The set up turned left or right depending on the relative orientation of the hinge actuators. The hinge actuators were the same as the ones used for rudder control. The hinge actuators are spring loaded so as to be self-centering, and try to maintain the insects aligned in place when turning motion is not required. In this technique, the moment can be increased by increasing the distance between the moths, thereby reducing the amount of turning needed, but at the cost of higher moment of inertia and hence slower response times. As mentioned above while applying a torque did change the orientation, the insect was able to quickly resist the applied force. However, the success of the navigational technique cannot be judged purely based on tethered flight, since it would be unreasonable to assume that the insect's orientation can be changed at will according to an external input. To check how effectively one can navigate the insect using each of the above mentioned techniques, untethered flight experiments were performed.

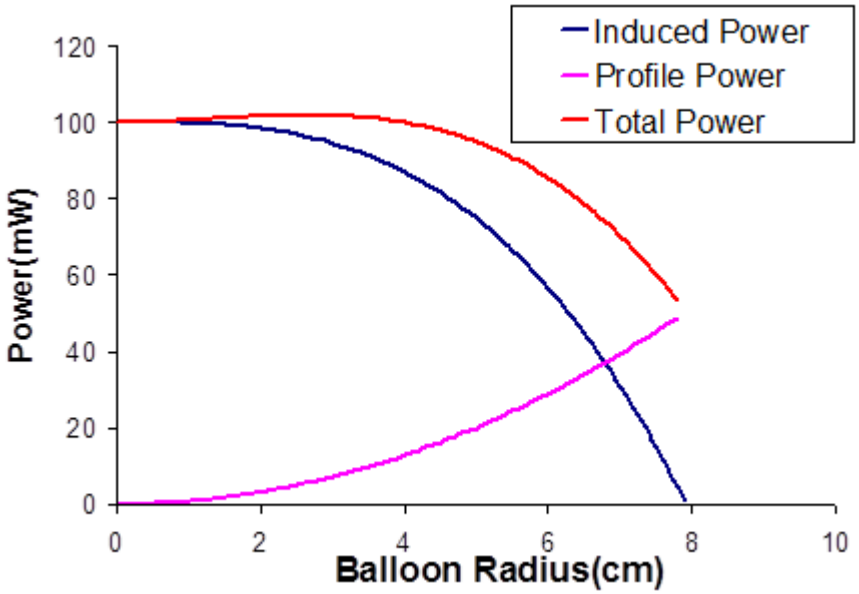

Figure 2.9: Power saving as a function of balloon radius

2.3.2 Balloon Tethered Flight

One of the challenges in realizing untethered flight is that the insects load carrying capacity is less than a gram. One way to conduct untethered flight experiments is using a Helium balloon for providing sufficient buoyancy to keep the backpack airborne. Here we discuss the modifications in the power requirements when using a balloon enabled IPMAV. Induced power (in mW/g) in all mechanical MAVs with dimension similar to that of a *Manduca Sexta* moth can be estimated by the formula [1].

$$P_{ind} = 14.0nR\left(\frac{\Phi C_L}{AR}\right)^{1/2} \tag{2.1}$$

$$P_{pro} = 18.2nR\left(\frac{C_{D,pro}}{C_L}\right) \tag{2.2}$$

Where n is the flapping frequency, R is the length of the wing, Φ is the angular displacement, AR is the wing aspect ratio, and C_L and $C_{D,pro}$ are the lift and profile drag coefficients respectively. Some power would also be needed to flap the wings, but in this case it can be neglected assuming that sufficient elastic energy can be stored so as to flap with negligible power. A Helium balloon can be used to provide sufficient lift. Using a balloon changes the power requirements, since while the balloon provides lift without power, it also induces drag at forward flight. So additional power is required at peak speeds while power saving is obtained at or close to hovering.

$$P_{ind}\text{reduction} = \Delta P_{ind} = 14.0nR\left(\frac{\Phi C_L}{AR}\right)^{1/2} \cdot \left(\frac{\text{Balloon Lift}}{\text{Mass without balloon}}\right) \tag{2.3}$$

$$P_{pro}\text{increase} = \Delta P_{pro} = 18.2nR\left(\frac{C_{D,pro}}{C_L}\right) \tag{2.4}$$

where C_D is the drag coefficient of the balloon and A is its area. Figure 2.9. shows a plot of the power saved during hovering flight and power needed during peak forward flight for a MAV calculated using Equations (2.3) and (2.4).

Type of Control	Actuator Used	Power Cons.	Effectiveness
Tail Motor	Plantraco 4 mm motor	1.0 W	Low, too disruptive, Insect turns about 90° after which insect resisted the motion consistently
Rudder	Plantraco, Microact Magnetic Actuator	20 mW	Low, Changes the direction to some extent but the force generated is fairly low
Differential Orientation	Plantraco, Microact Magnetic Actuator	20 mW - 100 mW	Fairly Effective

Table 2.2: Summary of flight control techniques and their effectiveness in tethered flight

The induced power reduces as a function of the volume of the balloon whereas the profile power increases as a function of the projected area. Hence, using a balloon results in power saving, but reduces stealth. When insects are used to power an MAV, external power is only needed for actuators to navigate the insect. Exact values of navigation power depend on the actuators used which will be elaborated in the later sections. When payloads used exceed that of insects lifting capability, balloon can be used to lift the excess payload. A balloon provides an excellent means of performing untethered flight experiments with large payloads without having to expend the power to keep it airborne. The same power savings apply while using balloon suspended insect MAV, as to a mechanical MAV (Figure 2.9).

MASS OF VARIOUS COMPONENTS		
Component	Weight in current backpack	Scalable to weight[]
Motor/ Actuator	0.8 g	<500 mg
Receiver	1 g	15 mg
Battery	.95 g	290 mg
Micsellaneous*	2 g	20 mg
Total	4.75 g	825 mg

* Includes glue, balsawood/carbon fiber used for assembly

Table 2.3: Mass of various components in the backpack.

2.3.3 Untethered Flight Control Experiments

For an IPMAV to be deployed for applications involving long range (~1 km) and long duration (~1-hr), it would be required that the insect always follow the external control and not fly erratically at any instant. It is also important that there is some control over elevation. Several different configurations were tried to achieve these characteristics. The following is a description of the experiments and the results for yaw control.

1. **Single moth balloon-tether flight:** Experiments were done to achieve long duration flight using a single moth in balloon enabled free flight. Control was attempted using two configurations, one using a tail motor and one using a rudder behind each wing (Figure 2.10E). As was observed in tethered flight experiments, the tail motor was very disruptive of flight and the moth would resist the applied moment. Slightly better performance was obtained using rudder behind each wing although the insect could still resist the applied moment. A typical flight trajectory is shown

in Figure 2.11. The points in the graph correspond to the position of the insect in intervals of 5 seconds. As shown, the insect has a tendency to change direction very often and fly without a particular target, almost resembling a two dimensional random walk [43]. Due to the lack of straight flight, external control was not very effective in making the insect fly long distance. The longest flight control distance obtained was 30 m realized in 5 minutes.

2. **Two moths balloon-tether flight:** Yaw control based on differential orientation was tried. A backpack was assembled using Plantraco micro actuators for left and right direction control. Each actuator when operated applied a moment of 15 gm-cm while consuming a current of 30 mA. A schematic of the experimental backpack is shown in Figure 2.10. The weight of various components used is given in Table 2.3. Since the weight of all components can be further scaled down in custom made designs, we also report the weight that can be attained in the final version of device. Over 0.6 km was achieved in about 40 minutes with two different test tracks with tolerable deviation from the desired path. A typical trajectory in two moth controlled flight in the corridor is shown in Figure 2.11.

3. **Three moths balloon-tether flight:** Experiments were done using three insects with independent control over orientation of the front and the back insects. The observed flight path was much straighter and navigation was relatively easier due to the straighter flight paths. For example, in an experiment about 1 km of flight distance was in 40 minutes, when only 0.6 km was achieved when using only two insects for the same time. These experiments suggest that adding insects tends to straighten out the flight enabling easier navigation.

4. **Roll based control of two moths:** Yaw or direction control was also attempted using roll control similar to that of an airplane. But it had little or no effect on the insect as the insect could easily change the stroke angles and offset the roll of the body.

5. **Elevation Control:** Elevation control was realized by changing the body angle of one of the insect in a two moth pair. The intention was to provide the system with a torque to change the pitch. But it did not result in a change of pitch, but rather the change in body angle provided additional force upward to obtain a gain in elevation. Similarly the system was made to lose elevation on demand and drop to the ground. In order to demonstrate pure elevation control without any forward flight, the system was spun by orienting the two insects relative to one another. Experiments were performed in a corridor with a ceiling of about 4 m and the system could be repeatedly made to gain or lose elevation.

2.3.4 Effect of Removal of Antennal and Visual Feedback

Sane et al.[44] have described the role of antennal mechanosensors in stabilizing flight of *Manduca Sexta*. It was shown that mechanosensory input from the antennae serves a role similar to that of halteres during flight in hawk moths. The antennae of flying moths vibrate and experience Coriolis forces during aerial maneuvers. The antennal vibrations are transduced by sensory organs at the base of their antennae in a frequency range characteristic of the Coriolis input. It was observed that removing the antennal flagellum of these moths severely disrupted their flight stability, but reattachment of the flagellum restored their flight control. Strange [45] discovered that visual feedback contributes toward

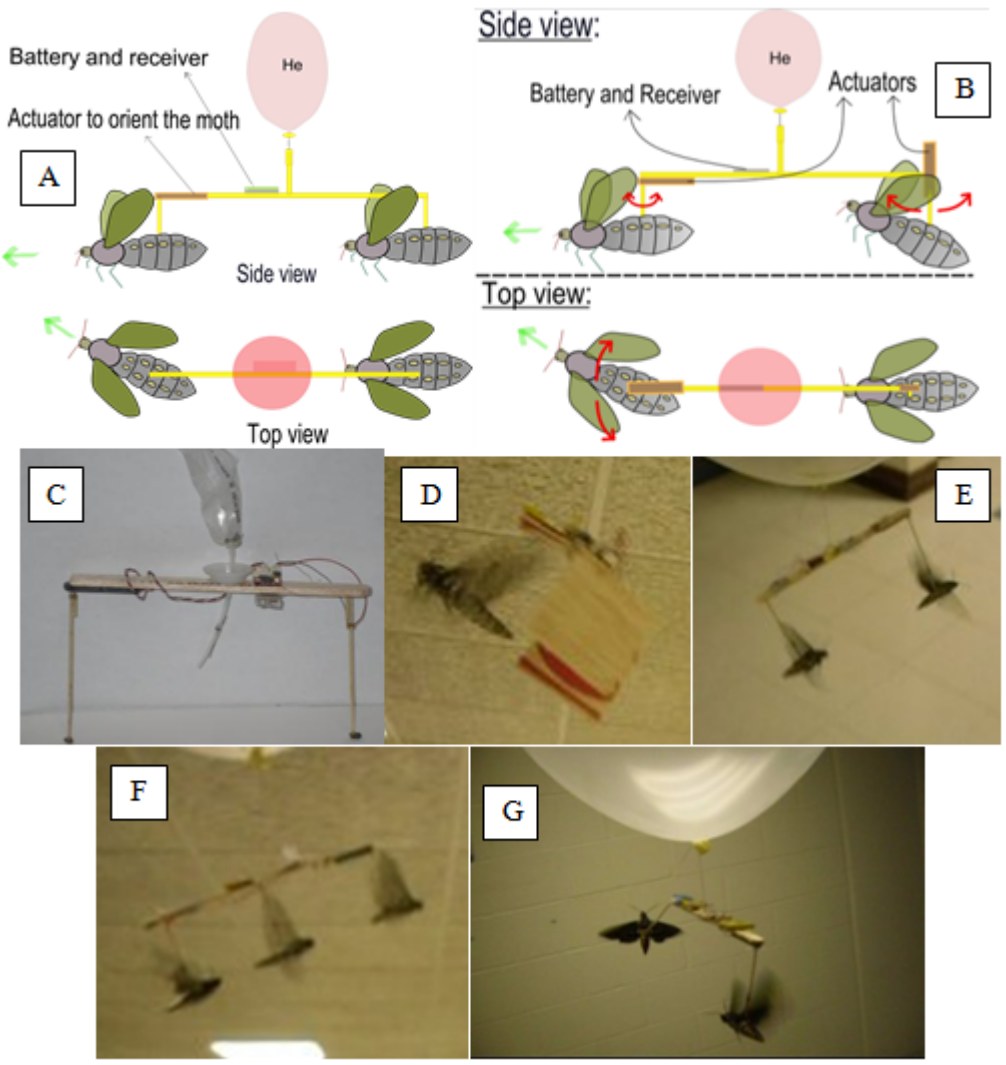

Figure 2.10: Schematic and Experimental setup of various untethered flight experiments. A, B: Schematic of Flight control mechanisms used. C: A backpack used in flight experiemnts, D, E, F, G: Various untethered flight configurations tried

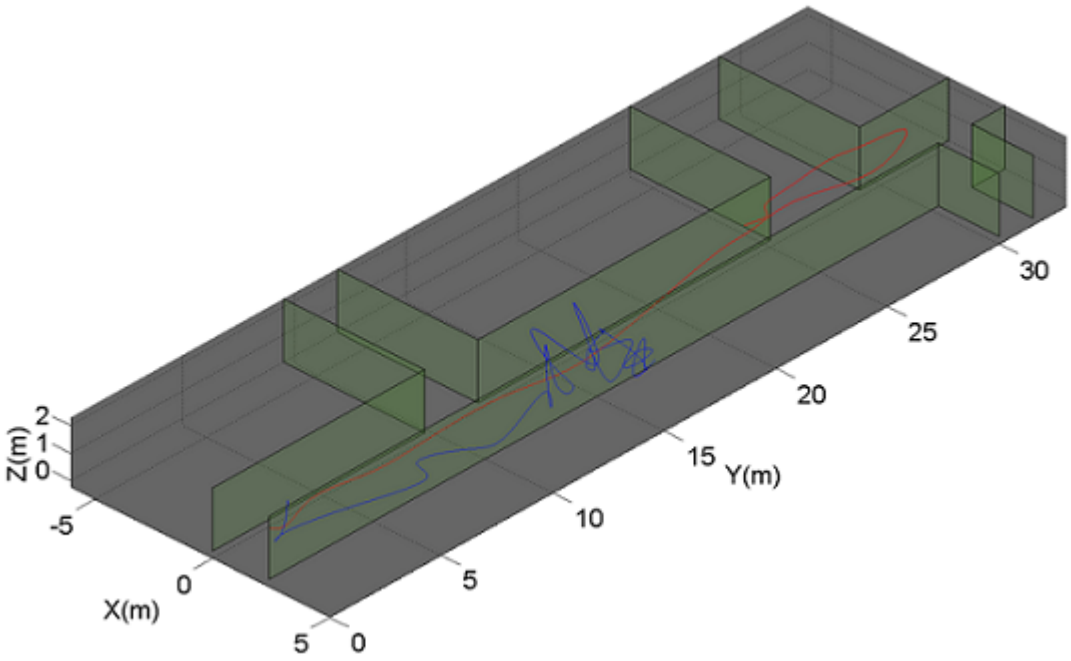

Figure 2.11: Flight trajectories of one moth vs two moth setup. As can be seen, in the system where we use two moths we have a straighter and more directional flight leading to quicker movement from start to end.

flight stability in dragonflies. Tethered flight and untethered flight experiments were performed to study whether removal of each of the feedback mechanisms would render the moth more responsive to external torque. Antennae were completely severed and the moth was placed inside an arena with constant visual stimulus ensuring that both the above mentioned feedback mechanisms were removed. The moth was steered in tethered flight using a rudder based mechanism. While it was possible to change the instantaneous orientation of the moth, continuous change was still resisted almost identical to that of a normal insect. Experiments in untethered flight where each of the above stimuli were removed independently also produced results similar to the ones where the insect's feedback sensors were kept intact. This might possibly be due to insect relying on multiple feedback sensors to stabilize flight.

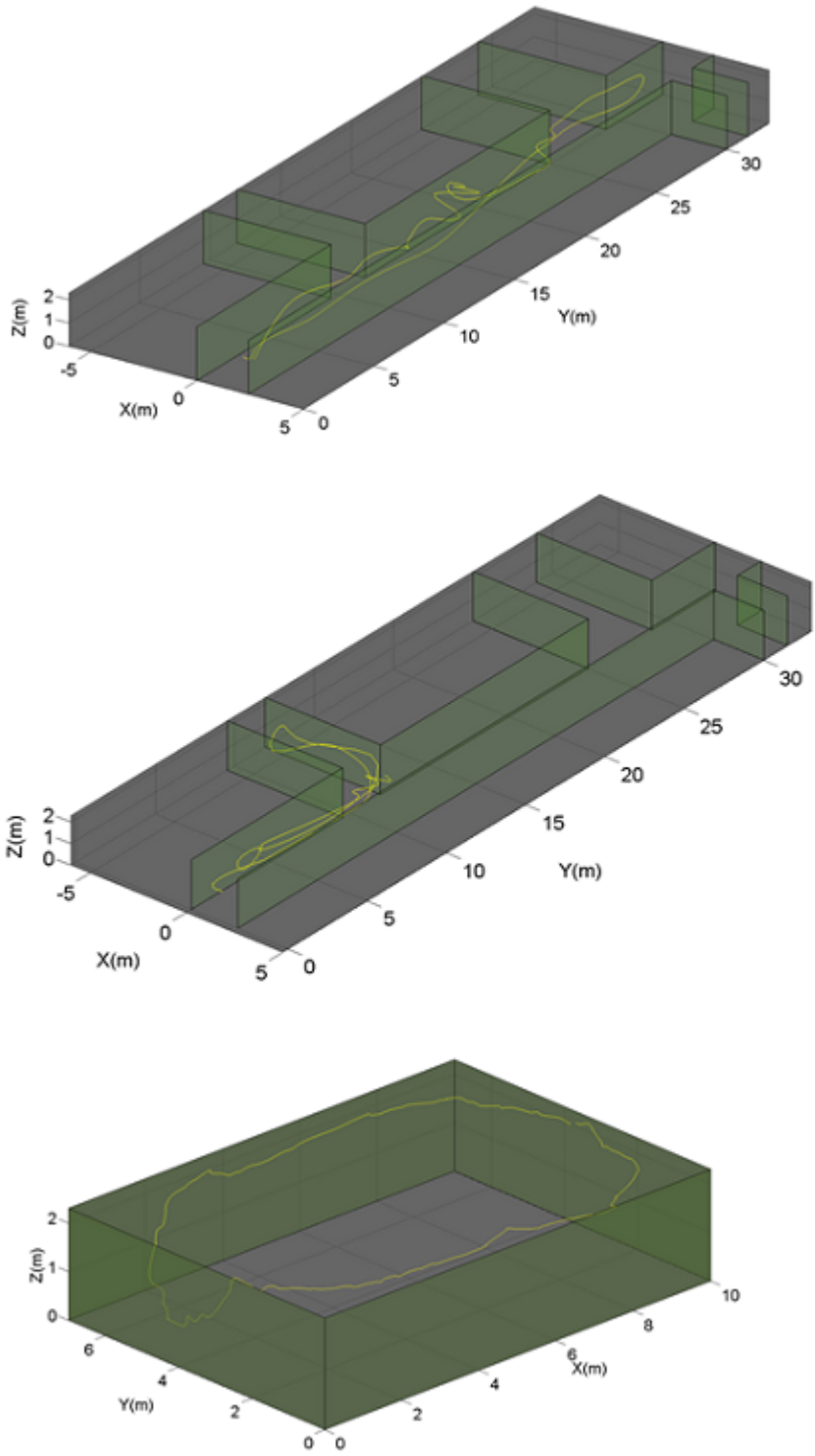

Figure 2.12: Figure showing various flight tracks and the trajectories observed with a two moth differential orientation control. As can be seen, the flight paths can be controlled with reasonable deviation from the desired path.1-km flight distance was obtained with all the trajectories.

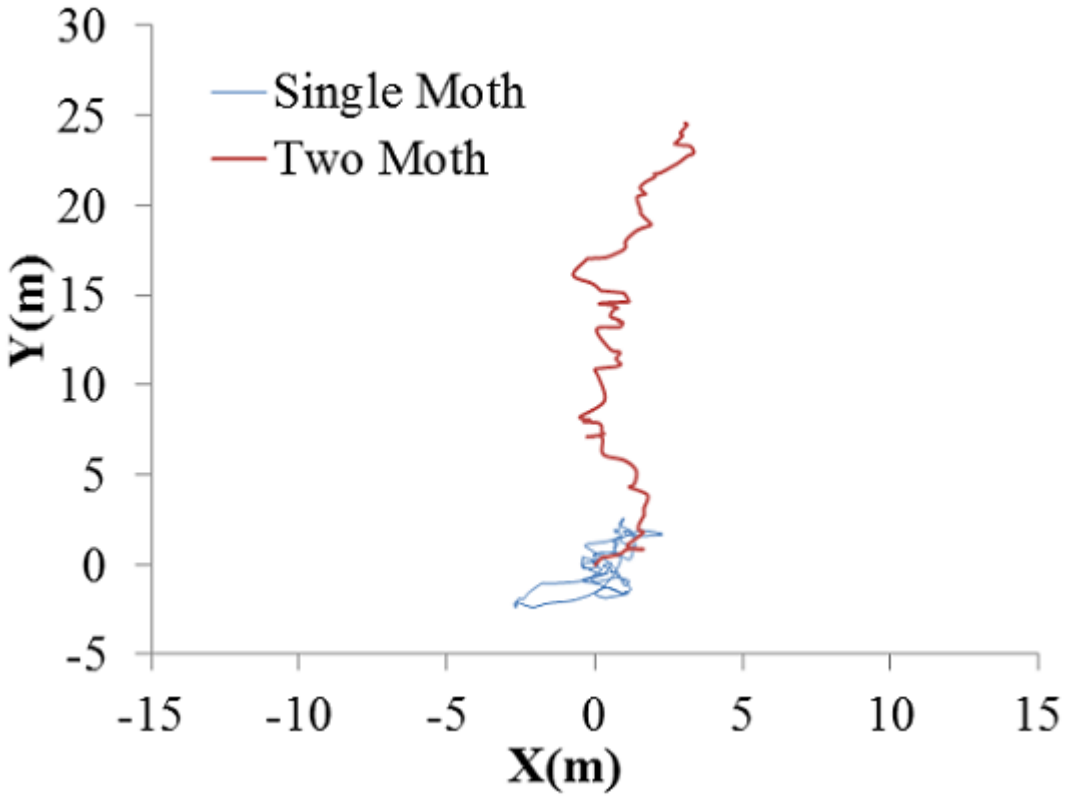

Figure 2.13: A: (Red): Simulated flight path with one insect. (Blue) Simulated flight path with two insects.

2.3.5 Tracks used and maximum flight distance achieved

We used three different set of flight tracks to perform long duration flight experiments. The flight distance targeted was about a kilometer. The test tracks are shown in Figure 2.12 along with the corresponding flight trajectories. The first one consists of a long corridor about 30 m long and 2 m wide. The moth was constrained to fly along the corridor back and forth till the total flight distance achieved was a 1 km. The second track was an L-shaped track with a length of 15 m and a width of 2 m. The moth was again made to go back and forth along the L-shaped corridor to achieve a total flight distance of 1 km. The third case was that of a large rectangular room with 10 m x 7 m in dimensions. Moth was

Configuration	Max controlled flight distance	Flight time
Single moth (rudder)	30 m	4 minutes
Two moths (differential orientation)	1 km	58 minutes
Three moths (differential orientation)	1 km	40 minutes

Table 2.4: Summary of the maximum flight control distance achieved with different configurations

controlled to go in a circle several times till the total flight distance added to 1 km. As can be seen, the flight was controlled along the desired trajectory with moderate deviation from the desired path. The summary of results is shown in Table 2.4.

2.4 Insect Flight Models

Insects are well known for their erratic flight that is composed of short straight paths that are intercepted by periods of rapid turns called saccades [43]. They are also known to be able to react rapidly to external disturbances [46]. While the control techniques that an insect employs and its reaction to external stimuli that result in these flight paths is a subject of much research, we use simple models to explain the observed experimental results.

2.4.1 Random Walk based model of flight

The flight of a single insect was modeled using a correlated random walk process as described in [43], where a single insect would fly forward for certain duration, then turn to some angle very rapidly and then repeat the same process again. The length of each move and the angle of turn are assumed to be independent random variables with the following probability densities:

- $p(l)dl$: the probability that the length of each flight has a value between l and l+dl
- $g(\theta)d(\theta)$: the probability that an angle between two consecutive flights measured clock-wise has a value between θ and $\theta + d\theta$

In the case of insects the distribution function of g(θ) is symmetric about zero since insects are equally likely to turn left and right and majority of the turns would be within 50 degrees. The flight of a two moths connected to each other would be different from a single one due to the fact that an attempt to change direction by either moth would have to alter the orientation of both the moths. Moreover the turning times may not coincide providing continuous forward flight. Saccades would not be as rapid due to higher moment of inertia which is about three orders of magnitude higher. This would produce only about one-tenth of a standard turn in one second. Hence the new turning angles were assumed to be only one tenth of the angles that a single moth would turn due to higher moment of inertia.

$$g_{new} = g_{old}(50 \cdot \theta) \tag{2.5}$$

Based on the new distribution, the path was computed and shown in Figure 2.13. As can be seen, for a given time, a system of connected moths is able to

achieve longer flight distances due to lesser randomness in their flight pattern.

2.4.2 Model of Insect Control System

Cohen et al. [46] developed a model for insect flight control system for a fruit fly based on a proportional derivative feedback. The governing equation for the dynamics is given by:

$$I\ddot{\psi} = \beta\dot{\psi} + N_{fly} + N_{ext} \tag{2.6}$$

where N_{ext} is the external disturbing torque and N_{fly} is the torque applied by the insect. It was observed that the feedback torque is very dependent on the angular velocity of the moth, which is given by:

$$N_{fly} = K_p\psi(t - \delta t) + K_D\dot{\psi}(t - \delta t) \tag{2.7}$$

This implies that if the angular velocity is small enough, which is the case in a two moth flier, the restoring force would be negligible preventing the autostabilizers of the insect.

2.5 Results and Discussion

The feasibility of balloon enabled insect powered MAVs for long duration flight missions have been demonstrated. Reliable means of aerial navigation have been proposed and techniques were developed to provide straight flight paths and minimize the erratic patterns of the insects. The mechanical force based flight control techniques demonstrated involves low-cost actuators. These provide striking advantages over purely mechanical MAVs. The proposed techniques are also not dependent on the insect which leads to the option of easily

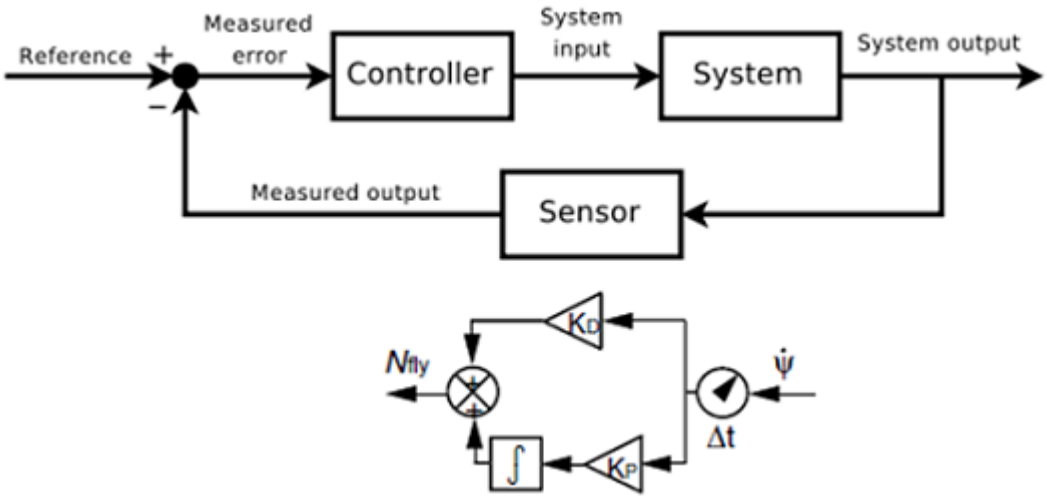

Figure 2.14: Figure shows the control model as has been proposed in Cohen et. al. The feedback sensors are primarily angular velocity sensors.

experimenting with any such insect and quickly coming up with an optimum solution.

CHAPTER 3

BALLOON INFLATION FOR INSECT POWERED MICRO AIR VEHICLES

3.1 Introduction

A balloon enabled IPMAV has several advantages as have been discussed in the Chapter 2. Balloon enables untethered flight experiments as well as provides power saving apart from the ability to be deployed from an airplane, by acting as a parachute to quickly reach a terminal velocity or to take-off from the ground and reach a certain height rapidly. Figure 3.1 shows the schematic of various stages of aerial deployment of a Balloon enabled IPMAV

- The balloon inflation backpack attached to the IPMAV is first dropped from an airplane.
- Next the balloon inflation mechanism would be triggered inflating the balloon.
- Once the balloon has been filled to satisfactory diameter, the balloon inflation mechanism would be ejected.
- The rest of the system would then be controlled to its desired destination.

In this chapter the efforts towards realizing an inflation backpack for the IPMAV are discussed. Lighter than air balloon inflation can be done using Hydrogen or Helium. While Hydrogen provides higher buoyancy due to its lower density relative to Helium and is relatively less expensive, it has the risk of ignition. While most applications do not require more than simple tank of Hydrogen or Helium used to inflate a balloon, two important efforts in the area of automatic

balloon inflators are described here. The first is using Calcium Hydride based Hydrogen generator for inflating weather/signalling balloons [47] and the other is development of Helium balloon inflator for Venus Vega mission [48]. Below we describe the details of techniques used in each of those efforts.

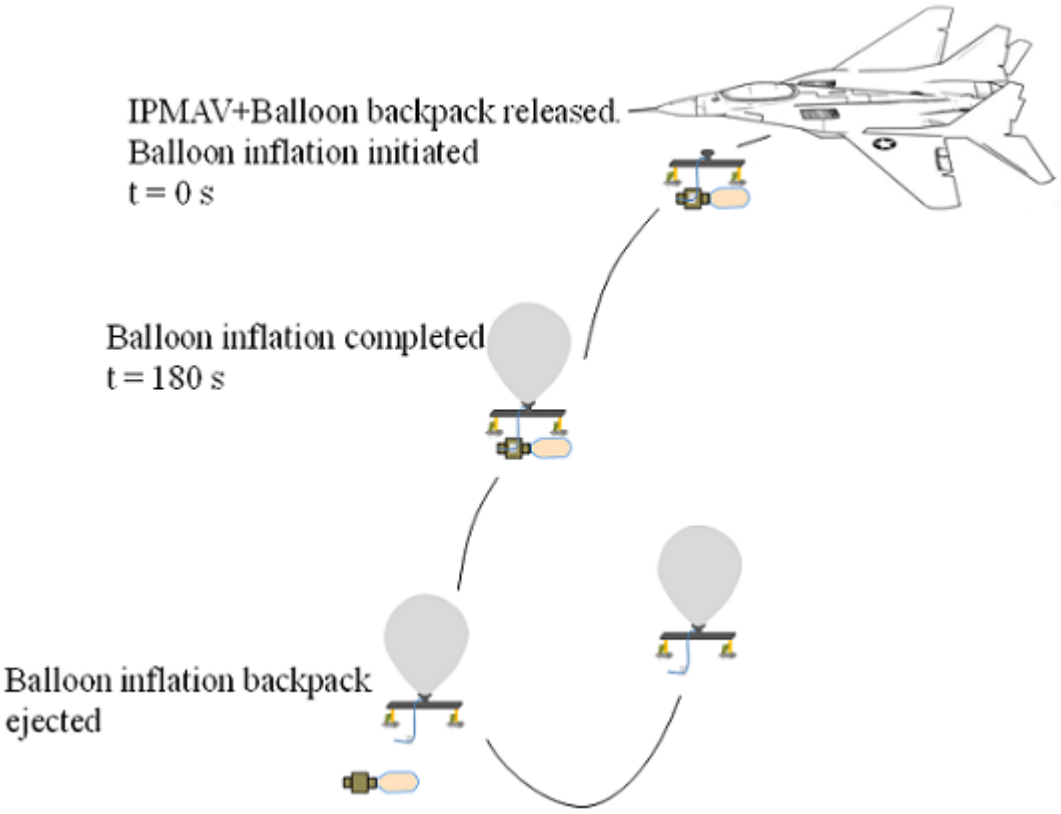

Figure 3.1: Schematic depicting the dropping and navigation mechanism of the insect

3.1.1 Venus Vega Balloon Deployment

Robotic Balloons or aerobots are an attractive method of planetary exploration. They could provide ultra-high resolutions of planetary surfaces especially for planets like Venus which is covered by thick clouds preventing observations of

the surface of the planet in detail. To study the surface of Venus in detail, in June 1985, two instrumented balloons were placed in the atmosphere of Venus as part of the VEGA mission. Figure 3.2 describes the deployment and inflation sequence. It also shows the entry capsule with various components including the entry parachute and the Helium tanks for balloon inflation. During the descent, the balloon was inflated to a pressure slightly greater than that expected at the float altitude with a predetermined quantity of Helium from tanks that were then jettisoned at an altitude of about 50 km. The Helium tanks were pressurized with Helium upto 30 MPa [48]. Each balloon had a nominal diameter of 3.4 m and supported a weight of 21.9 Kg and was designed for a float altitude of 50 Km.

3.1.2 Weather/Signal Balloon Inflation

Several Hydrogen generators have been patented since the 1940s for release of gaseous Hydrogen for balloon inflation. One of the widely used devices developed by the US Army in the 1950s is a balloon inflator using Calcium Hydride [48]. This has also been used for weather balloon inflation [49]. Figure 3.3 shows various components in a weather balloon inflation kit. This kit can be immersed in water to generate Hydrogen from a manifold that can be used to channel Hydrogen into the balloon. It consists of a Hydrogen generator, which is comprised of cylindrical steel can with an outlet tube attached to it. The bottom of the can is recessed and has a protruding center with interrupter threads for attaching the chemical charge. The bottom of the can also has a number of holes to allow water to enter the generator body. The generator set consists of a steel tube welded to a square sheet that has four holes for mounting the Hydrogen gen-

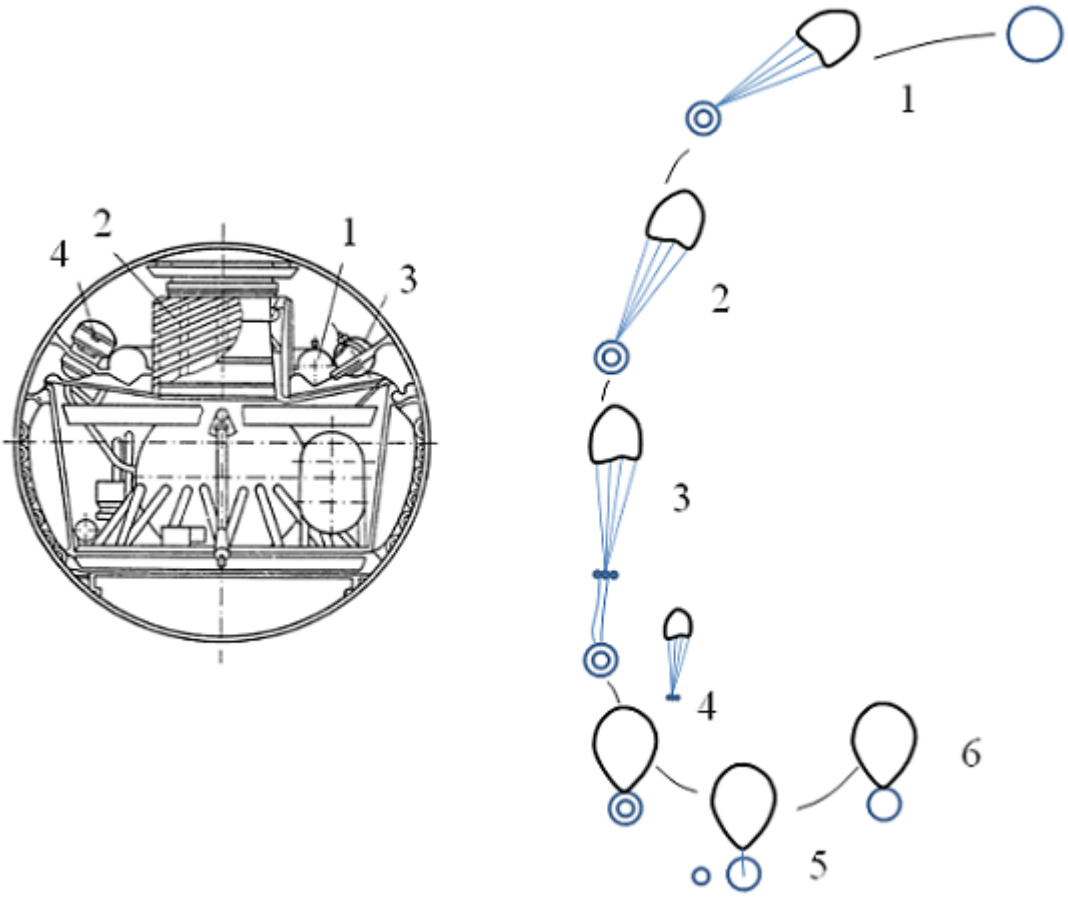

Figure 3.2: Schematic depicting the dropping and inflation of balloon. Left: Various components in the capsule - 1. Toroidal balloon compartment. 2. Lander transmitting antenna. 3. Helium Pressure vessel 4. Parachute compartment. Right: Various stages of the mission - 1. Venus atmosphere entry. 2. Parachute attached to landing cract opens. 3. Balloon probe released. 4. Balloon unfurls and inflates 5. Parachute and inflation system jettisoned. 6. Ballloon rises to its drift level

erators, short branch tubes connect hoses from each generator to the manifold. The Calcium Hydride charge is an airtight metal can containing approximately 6 ounces of 90-percent pure Calcium Hydride. The can is 3-3/4 inches in diameter, and 2 inches high. The top of the can is recessed and is provided with interrupted threads for attaching the charge to the bottom of the generator body. On the top of the can there are a number of knockouts that can be removed to allow water to enter the can. The charge will produce approximately 6 cubic feet of Hydrogen for inflation of a 30-gram balloon when the generator set is immersed in water.

3.2 Balloon Inflation Experiments

Three distinct strategies for balloon inflation were identified. Firstly one can use the expansion ratio of liquid Helium (757:1) to realize a high pressure Helium container that can be later released producing sufficient Helium to inflate a balloon. The second technique is using a container that can mix Calcium Hydride and water on demand to release Hydrogen to inflate a balloon. Thirdly it was based on a commercial Helium vessel to inflate a balloon. They are described in detail below.

3.2.1 Using Liquid Helium Expansion Ratio

High pressure Helium can be generated using expansion ratio of Liquid Helium. Liquid Helium boils at a temperature of 4 K. The expansion ratio of 1 liter of liquid Helium is 757 resulting in 757 liters of room temperature Helium

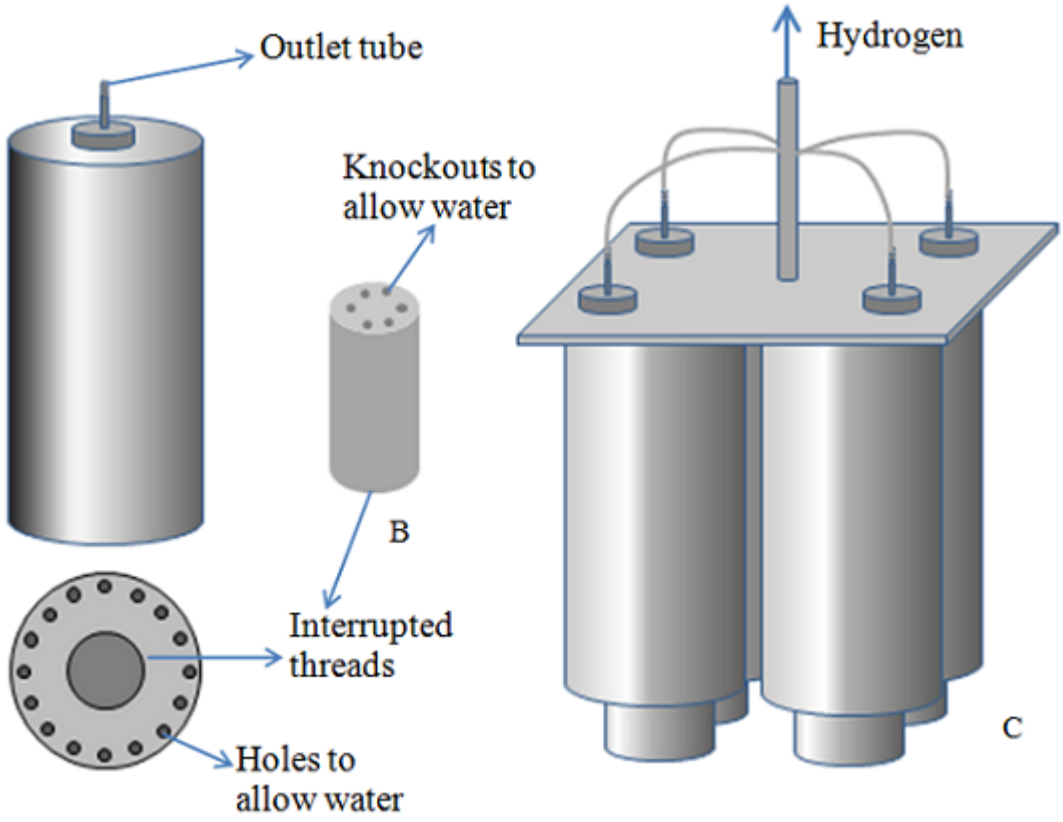

Figure 3.3: Hydrogen generator that consists of a cylindrical steel can the bottom of which is equipped with interrupted threads to attach a chemical charge (B). The bottom also has a number of holes to allow water to enter into the generator body. B: Chemical charge containing Calcium Hydride (CaH_2). The top of the can has a number of knockouts that can be removed to allow water to enter into the body of the can. C: Hydrogen generator set that consists of four Hydrogen generators and Calcium Hydride charges. This setup can be immersed in water to generate Hydrogen that can be used to inflate a balloon.

gas at atmospheric pressure (STP) when 1 liter of liquid Helium is allowed to evaporate. One of the main challenges in realizing the expansion ratio inside a closed system is finding low temperature seals. Below -150°C , low temperature crystallization causes rubber materials to become brittle rather than elastic rendering them ineffective as seals in such a state [50]. Indium has been used as a successful seal for low temperature vacuum experiments [50]. For realizing the expansion ratio, indium was used as a cryogenic seal. Experiments were performed on a liquid nitrogen bath (Figure 3.3). A 1-cc volume pressure vessel (Figure 3.4) was used to test the percent of expansion ratio that is practically realizable. Since Liquid nitrogen (LN) has a boiling point of 77 K, experiments were done with LN. The pressure vessel was immersed in LN and was held tightly with a pair of tongs. The hexagonal bolt equipped with indium seal was tightened onto the vessel using a socket wrench. This ensures that there is minimal evaporation during the process of tightening leading to very little loss of LN. The vessel was removed from the bath while still applying torque on the bolt to account for warming up of the pressure vessel. Eventually when room temperature is reached, the vessel was weighed and the difference between the mass of the vessel before and after the filling gives the mass of Nitrogen trapped in the vessel. A trapped mass of 235 mg was obtained which corresponds to about 183 ml of STP N_2, resulting in a realized expansion ratio of 183. This is consistent with the results reported earlier [50].

3.2.2 Hydrides for Balloon Inflation

Metal hydrides are promising materials as a storage medium for Hydrogen, often reversibly [51]. Their high Hydrogen content (7-11% by weight [51]) makes

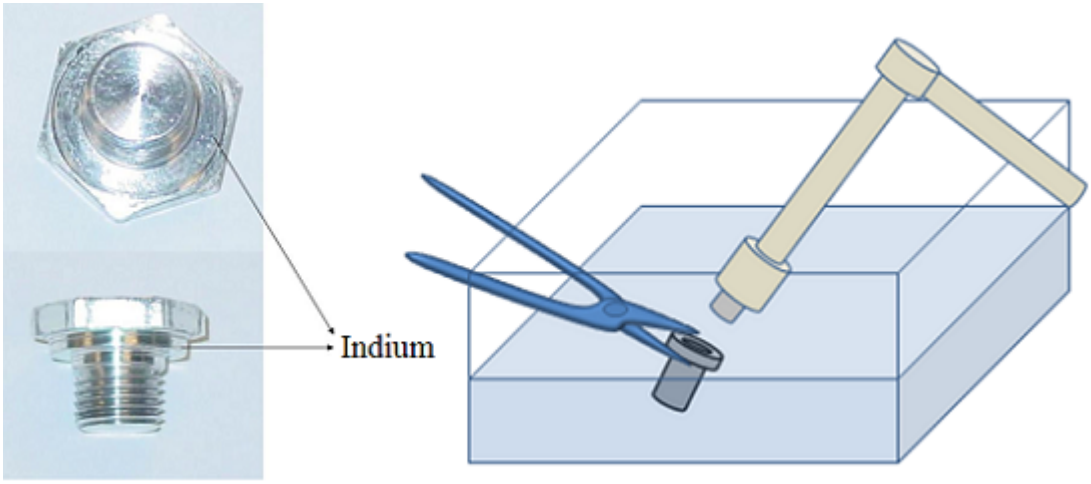

Figure 3.4: (Left) The pressure vessel cap is fitted with indium rings for low temperature sealing. (Right) Pressure vessel being fitted with the seal in a liquid nitrogen bath.

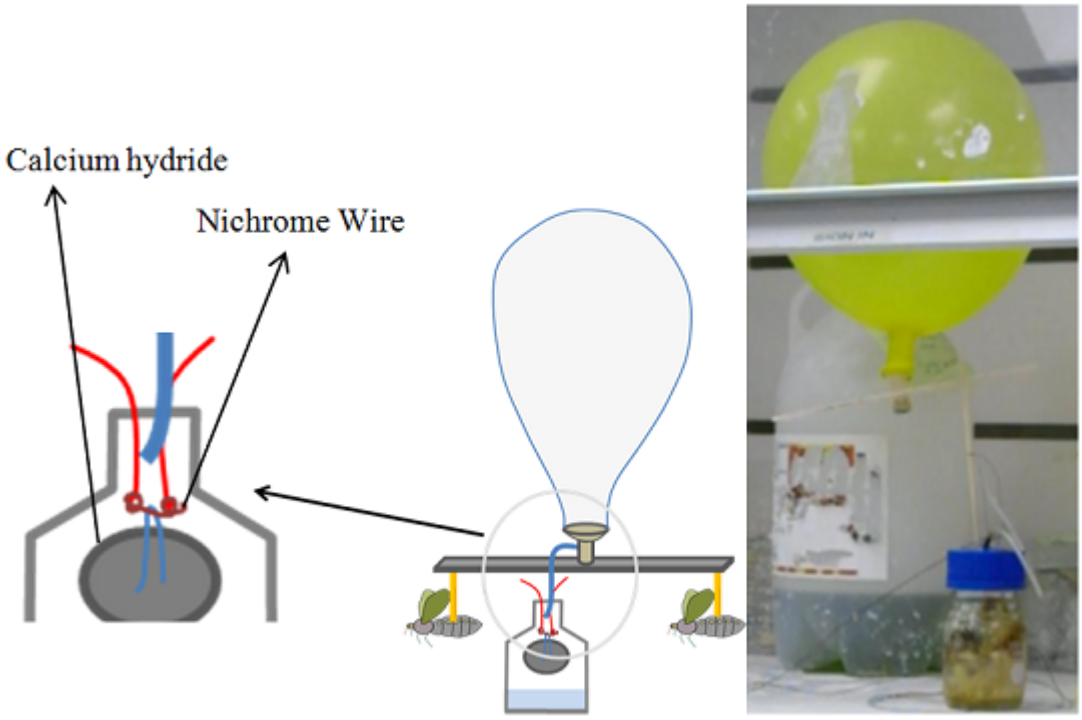

Figure 3.5: (Left) Schematic of Hydride balloon inflation. (Right) Figure shows the set up of the reaction chamber and the inflated balloon.

them potential Hydrogen storage medium for future fuel cell powered vehicles. Proposed hydrides for use in a Hydrogen economy include hydrides of Magnesium (MgH_2) or transition metals and complex metal hydrides, containing Sodium, Lithium, Calcium and Aluminum or Boron. Hydrides chosen for storage applications provide low reactivity with air at room temperature (and thus high safety) and high Hydrogen storage densities. Balloon inflation for IPMAV involves the need to inflate a few liters of Hydrogen on demand. Since hydrides react readily with water, their reaction with water was chosen as the means to generate Hydrogen. Magnesium Hydride (MgH_2), Lithium Aluminum Hydride ($LiAlH_4$), and Calcium Hydride (CaH_2) were tried and CaH_2 was identified as the optimum method for the release of Hydrogen into a balloon. While the $LiAlH_4$, MgH_2 were tried, $LiAlH_4$ reaction with water was too exothermic for the balloon to withstand such high temperatures and MgH_2 reaction was too slow and it took a very long time to inflate the balloon. The set-up of the experiment is shown in the Figure 3.5. It consists of a glass tube with 10 ml of water and Hydride is suspended in air. Hydride could be made to react with water by dropping the hydride using a Nichrome Wire. The Hydrogen generated from the reaction is then channeled into the balloon using a tube that then feeds the gas into the balloon via a one way valve. The volume of the Hydrogen generated was about 5.5 liters in 2 minutes.

3.2.3 Helium Pressure Vessel

A commercial Helium vessel can be used to inflate a balloon. However commercial pressure vessels are typically less than 3000 psi due to safety concerns. Thus the volume of such a vessel used to inflate a Helium balloon can be signif-

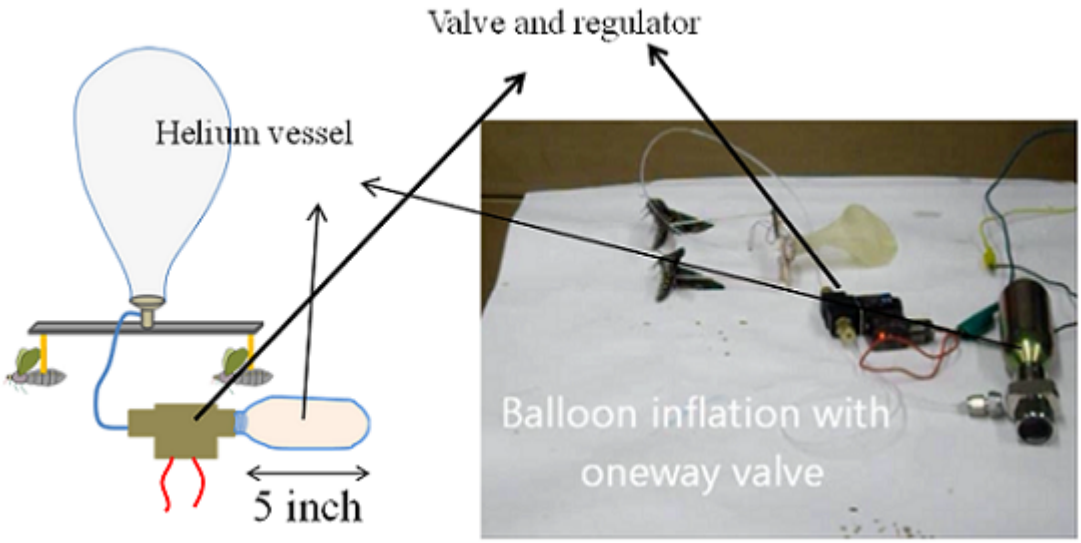

Figure 3.6: (Left) Schematic of balloon inflation. (Right) Shown is the Helium pressure vessel with regulator and valve and the balloon inflation setup with insects

icant. A Leland Helium cylinder (Catalog number 49615He) with a pressure of 2500 psi containing 13.5 liter Helium was used as the Helium source. A Leland Helium Regulator (50047-004) was interfaced to reduce the outlet pressure to 80 psi and a Direct Acting Normally closed Two Way Solenoid Valve (12 V DC) was used to release the pressure (Figure 3.6). The balloon could be inflated by releasing the pressure in the vessel with the solenoid valve. Once the balloon was inflated to satisfactory diameter, the valve was closed and the connecting tube was severed with a heated Nichrome wire.

3.3 Conclusion

The possible techniques for realizing an automatic self-contained balloon inflation mechanism were examined. The technique involving a 2500 psi Helium vessel used with a regulator and a valve was identified as the most optimal way

of inflating the Helium balloon in terms of consistency, safety and portability. The inflation setup could be detached from the insects using a Nichrome wire to severe the tube. Hence this technique enables deployment of the Balloon Enabled IPMAV without human intervention. Consequently, the current work leads us towards realizing the benefit of IPMAV without any human intervention.

CHAPTER 4

CENTIMETER SCALE HIGH ENERGY DENSITY PRESSURE VESSEL

4.1 Introduction

MEMS actuators require mechanical actuators with high energy and power densities to enable high force and mechanical power output even as the dimensions of the devices are shrunk to mm and micro-scales. Most actuators (electrostatic, piezoelectric, thermal, and shape memory alloys) rely on electrical power to generate forces. And, in many applications such as micro-scale robotics, the battery powered actuator has to move not just the payload and frame of the robot, but also the battery that powers the actuators. The conversion efficiency of electrical to mechanical energy can be high for macro-scale engines, but at MEMS scale, few actuators are above 10% efficient, due to high voltage needed and inertial friction forces [52]. Hence, one can save volume and energy - carrying capability by developing a power source that generates mechanical power directly rather than using electrical power as an intermediate storage path. When the energy storage elements are mechanical, the conversion of stored mechanical energy to usable mechanical power is direct, and efficiencies can be potentially 100%. Mechanical energy can be stored either in springs in the form of elastic energy stored in mechanical components, or as the compressed energy in gases (Pneumatic). While electrostatic and electromagnetic actuators remain popular in MEMS, recent research revealed that pneumatic actuators develop higher force and power density at microscale [52]. Pneumatic power sources offer several advantages creating unique opportunities for Microsystems:

1. Reduction in overall system weight and volume: eliminating the battery

volume needed for the actuator reduces the required total power density.

2. Wider temperature compatibility: High pressure storage systems do not suffer from temperature activated chemical processes, enabling power sources that could operate from cryogenic to 200-300°Celsius.
3. Generation of high pressure flow: The miniature pressure vessels enable very high pressure or flow output for very high instantaneous power output.

Applications for these actuators exist in fields ranging from microfluidics and BioMEMS to microrobotics. MPVs can also be used in the domain of MEMS gas based devices such as micro gas analyzers, micro-fluidic pumps, and micro cryogenic coolers. The compressed gases can be used to create pumps using the venturi effect and to cool substrates using the Joule-Thompson expansion effect. Other applications include micropropulsion devices that produce large amounts of thrust by releasing high pressure gas rapidly. Actuators at micro scale using varying degrees of pressurized air/liquid as a power source typically occur in the following categories:

- Elastic Membrane Actuators: Elastic or flexible actuators comprise at least one component that deforms elastically under the applied pressure [53, 54].
- Piston Cylinder Fluidic Actuators: While Piston cylinder mechanism is challenging to fabricate on a micro-scale due to low friction sealing requirements, they are not entirely uncommon [55, 56].
- Drag based fluidic actuators: They make use of drag force between the fluid and the actuator [57, 58].

4.2 Power and Energy Density of Pneumatic Sources

Pneumatic power sources are an attractive alternative to conventional battery at small scale due to several reasons. Firstly, pneumatic power sources can have comparable energy density to Lithium batteries partly made possible by advances in composite technology achieving unprecedented strength to weight ratios [59] and partly due to 100% conversion efficiency. Secondly, the stored energy can be released very quickly or very slowly spanning a wide range of operation on the power density scale. The following section provides a comparison between the Energy density of Pneumatic actuators and the traditional Lithium Batteries.

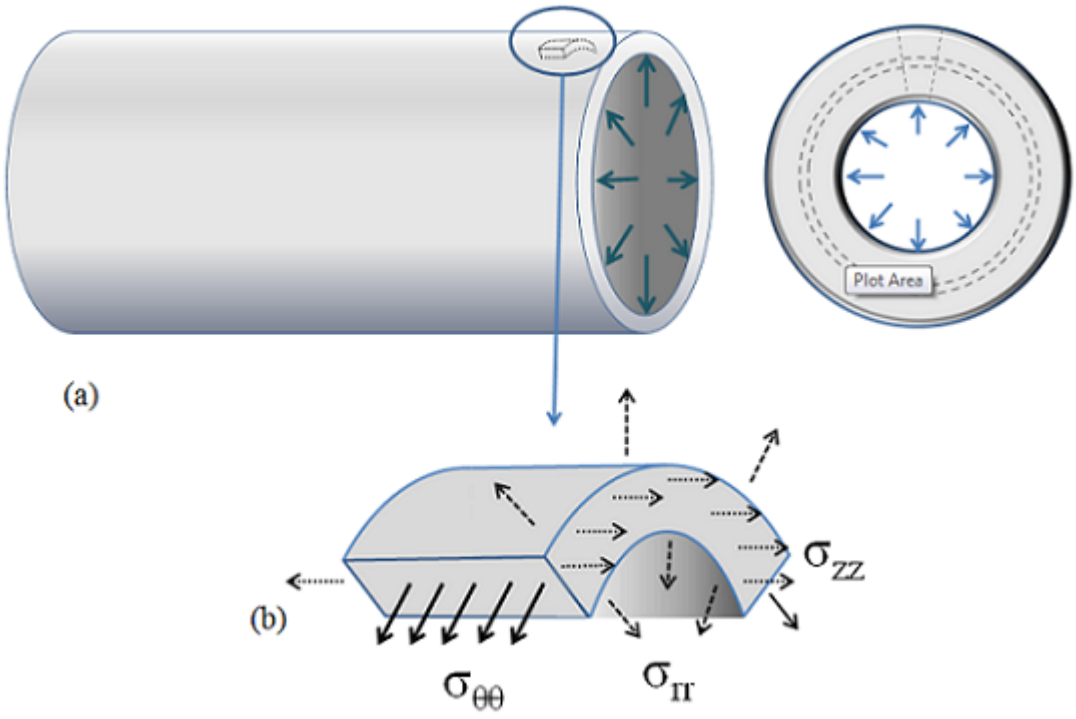

Figure 4.1: (a) Cross-section of thick walled pressure vessel with inner radius r_i and outer radius r_o. (b) inset showing radial and hoop stresses acting on an pressure vessel wall element.

4.2.1 Pressure-Vessel Stress Analysis

The maximum energy that can be obtained from a compressed gas at a pressure P_A, temperature T_A and occupying a volume V_A using an isothermal process is given by:

$$W_{A\to B} = nRT \ln\left(\frac{P_A}{P_B}\right) = PV \ln\left(\frac{P_A}{P_B}\right) \tag{4.1}$$

where P_B is the atmospheric pressure and PV is the pressure volume product which is invariant between the initial and final state. The details of the derivation are given in appendix A. This amounts to about $2.271ln(P_A/P_B)$ kJ at 0°C (273 K) or 2.478 $ln(P_A/P_B)$ kilojoules (kJ) at 25 C (298 K), per mole, or simply 100 $\ln(P_A/P_B)kJ/m^3$ of gas (at atmospheric pressure). Thus, the maximum energy density of pneumatic sources is directly related to the burst pressure of the source and the mass. Consider a cylinder of inside radius r, outside radius R, and length L containing a fluid under pressure p. The following set of equations describes the equilibrium elasticity equations in polar coordinates assuming the cylinder is sufficiently long to describe the equilibrium equations in 2 dimensions.

$$\frac{\partial \sigma_r}{\partial r} + \frac{1}{r}\frac{\partial \tau_{r\theta}}{\partial \theta} + \frac{\sigma_r - \sigma_\theta}{r} = 0 \tag{4.2}$$

$$\frac{\partial \tau_{r\theta}}{\partial \tau} + \frac{1}{r}\frac{\partial \sigma_\theta}{\partial \theta} + 2\frac{\tau_{r\theta}}{r} = 0 \tag{4.3}$$

where σ_r and σ_θ are the radial and hoop stresses respectively. These equations need to be solved along with appropriate boundary conditions which can be given at the inner and outer surfaces as follow:

$$\sigma_{rr} = \sigma_{r\theta} = 0 \text{ on } r = r_o \tag{4.4}$$

$$\sigma_{rr} = -p, \sigma_{r\theta} = 0 \text{ on } r = r_i \tag{4.5}$$

Among hoop stress, longitudinal stress and bending stress, hoop stress is twice the other two stresses and the pressure in the hoop stress corresponds to burst pressure when hoop stress reaches ultimate tensile strength. The burst pressure of a pneumatic cylinder of wall thickness t and radius r made out of a single material is given by:

$$P_{burst} = \frac{2t}{r}\sigma_{ult} \tag{4.6}$$

where σ_{ult} is the ultimate tensile strength of the material constituting the vessel.

4.3 Composite overwrapped pressure vessels

Composite materials are materials formed from two or more elements with significantly different physical or chemical properties from its constituents. Typically, composite material is formed by reinforcing fibers in a matrix resin. The reinforcements can be fibers, particulates, or whiskers, and the matrix materials can be metals, plastics, or ceramics. The fibers carry the load and provide structural properties to the composites. The matrix materials serve to bind the fibers together and transfer the load to the fibers apart from providing required surface finish quality. Examples of composite materials include wood, fiber reinforced polymers, carbon or glass reinforced plastics etc. [60]. A composite overwrapped pressure vessel (COPV) consists of thin metal liner wrapped with high strength fiber or polymeric matrix resin designed to hold fluid under pressure. The metal liner acts as a barrier preventing leaks and chemical degradation of the structure. The stresses are carried by high strength, low density composite. The most common liner materials are Aluminium, Titanium, Inconel alloys and Stainless steels while the composites used generally are fiber reinforced polymers (FRP) using carbon and Kevlar fibers. Some matrix resins

that are in use are epoxies, isocynate-base polymers polyimides. The primary advantage of a COPV as compared to similar sized metallic pressure vessel is better strength to weight ratio. The fabrication of a COPV involves winding the composite material over the liner using a filament winding machine that wraps composite around the liner along a desired orientation.

The applications of COPV are primarily based in aerospace industry especially in high pressure applications. COPVs have totally replaced monolithic Titanium vessels for applications involving pressurized tanks for chemical propulsion systems, Gas-supply tanks for inflation systems, science instruments etc., xenon propellant tanks for electric propulsion systems etc. They are also used in launch vehicles, earth orbiting and planetary spacecrafts[61].

4.3.1 Composite vs. Metal Pressure vessel analysis

The cross-sectional stresses for a thick-walled vessel are shown in Figure 4.1. For a pressure vessel wrapped in composite, assuming thin walled pressure vessel equations hold, the burst pressure is given by:

$$P_{burst} = \frac{\sigma_{metal}}{r} t_{metal} + \frac{\sigma_{composite}}{r} t_{composite} \tag{4.7}$$

This would imply that for modern composite based materials, the burst pressure would be significantly higher than that of Pure Metal liners. Table 4.1 shows the comparison of strength and density of various composites and metals. As can be seen, for modern composite materials, the burst pressure would be significantly higher than that of pure metal vessels.

Based on these calculations the energy density of composite based pnuematic sources was computed and plotted Figure 4.2 and Figure 4.7. As can be

Material	Ultimate Strength(MPa)	Density (g/cm^3)	Specific Strength (kN-m/kg)
Aluminum alloy	600	2.7	222
Steel alloy	2000	7.86	254
Titanium alloy	1300	4.51	288
Glass fiber	3400	2.6	1307
Carbon fiber	4300	1.75	2457
Carbon nanotube	62000	0.037-1.34	46,268-∞

Table 4.1: Table shows various materials and their corresponding specific strength. Composite fibers are shown in bold.

seen the energy density of pneumatic sources can be increased almost by a factor of two to three by using composite materials. The basic design method is to orient the fibers in the direction of the principal stresses and proportion to the number of fibers with respect to the size of the principal stresses. In structures where it is geometrically impossible to orient the fibers precisely in the direction of the principal stress they are oriented at some angle with it. A balanced structure can be achieved by proportionately locating fibers at two basically different winding angles (low helicals and circumferentials). The balanced structure is one in which the fibers oriented in any direction in the structure have equal stress applied to them under load. Three basic patterns have been developed and used by industry to produce filament-wound structures, namely, circumferential winding, helical winding and polar winding. Each winding pattern can be used alone or in various combinations, in order to provide different structures (Figure 4.3).

- **Circumferential Winding:** This pattern basically involved the circumferential winding at approximately a 90-degree angle with the axis of rota-

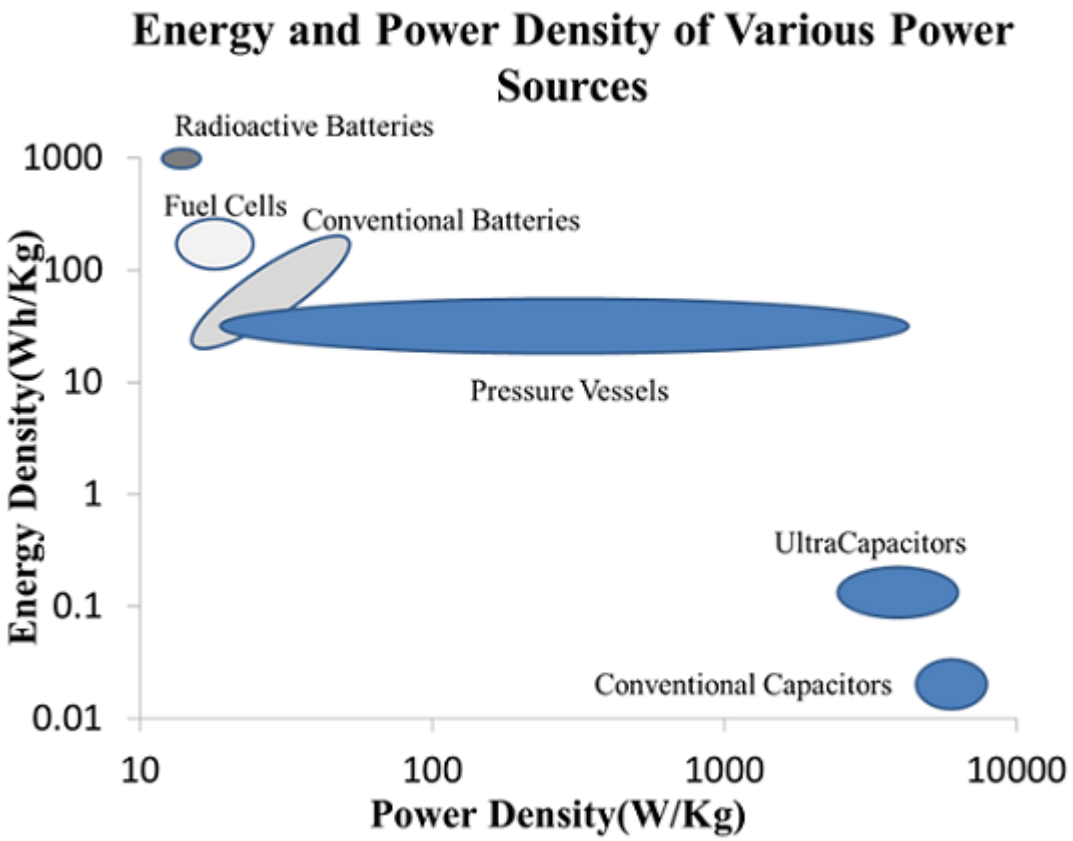

Figure 4.2: Energy density of pneumatic sources vs other energy sources.

tion, interspersed with longitudinal reinforcements. Maximum strength is obtainable in the hoop direction. This type of pattern generally does not permit winding of slopes over 20° when using a wet winding reinforcement or 30° when using a dry winding process. It also does not result to the most efficient structure when end closures are required. With end closures and/or steep slopes, a combination of helical and circumferential winding is used.

- **Helical winding:** The reinforcements are applied at any angle from 25° to 85° to the axis of rotation. No longitudinal filament need be applied, for low winding angles provide the desired longitudinal strength as well as the hoop strength. By varying the angle of winding, many different

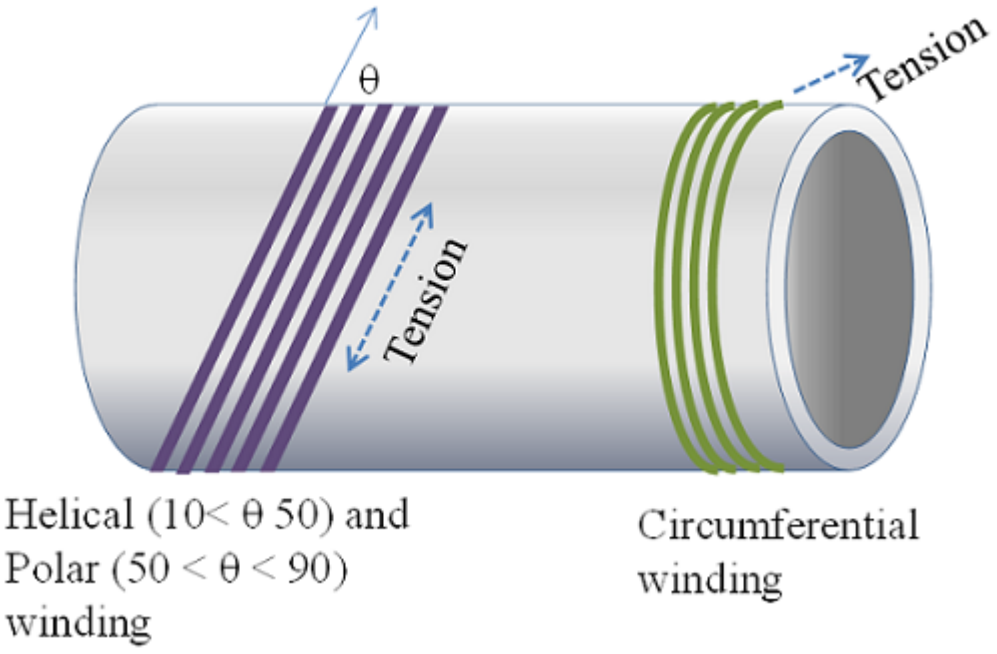

Figure 4.3: Figure shows Polar, helical and circumferential windings and the direction of tension acting on the fibers.

ratios of hoop to longitudinal strengths can be obtained. Two different techniques of applying the reinforcement in helical windings are used by industry. One technique is the application of only one complete helical revolution around the mandrel from end to end. The other technique involves a multicircuit winding procedure, which permits a greater degree of flexibility in angle of wrapping and length of cylinder.

- **Polar Winding:** In polar winding, the fiber passes tangentially to the polar opening at one end of the chamber, reverses direction, and passes tangentially to the opposite side of the polar opening at the other end. In other words, fibers are wrapped from pole to pole, as the mandrel arm rotates about the longitudinal axis as shown in Figure 4.4. It is used to wind almost axial fibers on domed end type of pressure vessels. On vessels with parallel sides, a subsequent circumferential winding would be done.

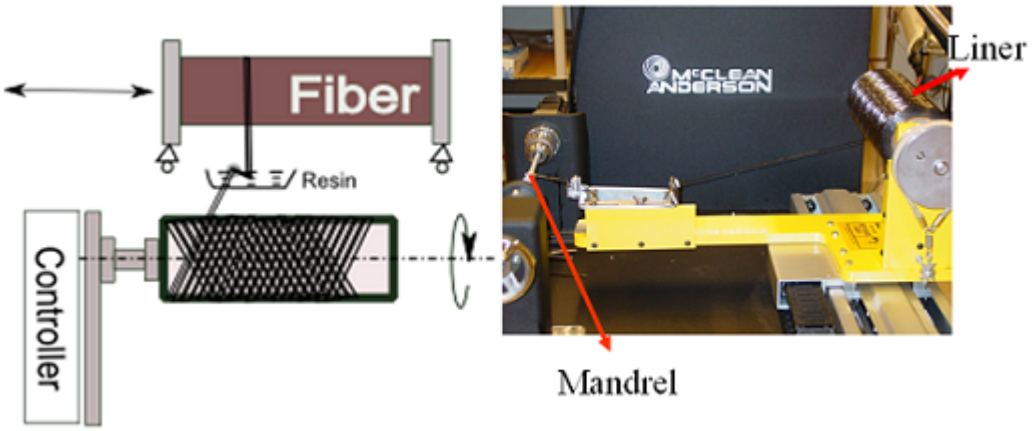

Figure 4.4: (Left) Schematic of the winding process in the filament winding machine; The mandrel rotates, winding the fiber around the liner. The stage moves to position the fiber along the liner. (Right) Filament winding machine setup.

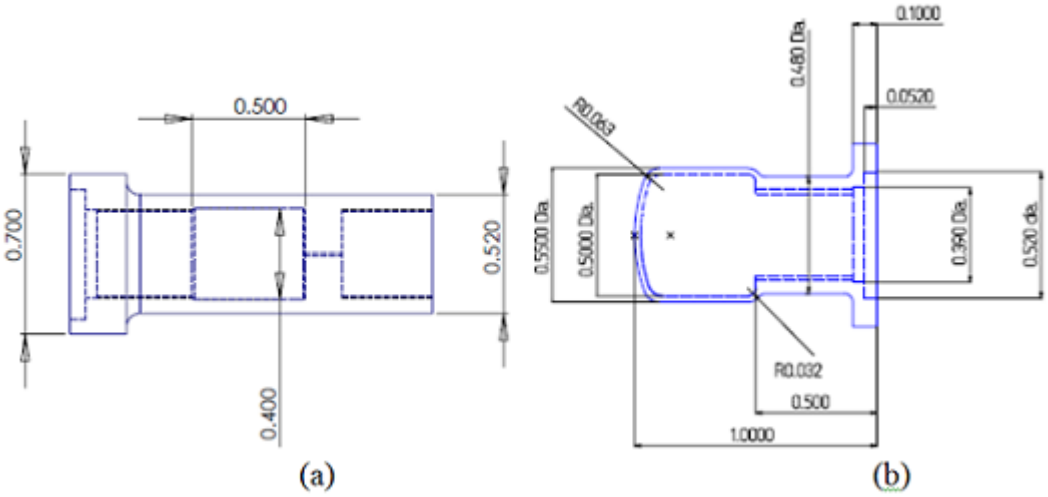

Figure 4.5: CAD model of the Aluminum liner with (a) opening on both sides, one for filling high pressure fluid and other for interfacing with high pressure valve, (b) opening on only one side.

4.3.2 Design and Experimental Testing of Wound Pressure Vessels

Realizing a Centimeter Scale High Energy Density Pressure Vessel (CSHPV) involves several steps. Firstly, the liner has to be designed to obtain the desired base burst pressure. The material also has to be easily machined, with a reasonably high strength to weight ratio. Secondly, the liner has to be wrapped along a particular orientation with the composite fiber for maximum strength. Lastly the finished CSHPV has to be tested for realizable burst pressure and consistency. **Design of Liner:** Several liners were designed and tested to obtain optimum weight to burst pressure ratio. In view of performance Aluminum 7068 alloys were selected for a mix of machinability, strength to weight ratio and cost [62]. A CAD drawing of the liner is shown in Figure 4.5(a), Figure 4.6. The liner was designed with an inner diameter of 0.4 inches and an inner volume of 1 cc, and a mass of 8 grams. The liner was designed to provide a burst pressure of 2000 bar without any overwrap. The liners were machined at a commercial machine shop . As can be seen in Figure 4.9, the basic design involves a cylinder with threads on either side. The cylindrical design enables ease of manufacturing and subsequent wrapping. Both sides are threaded to facilitate filling of high pressure fluid on one side and controlled release using a valve interface on the other side. **Fabrication:** Fabrication of CSHPV was performed using a McClean Anderson Filament winding machine two axis machine with a rotating mandrel and a moving carriage to move the fiber position along the mandrel. Toray T1000G Fiber, which has a tensile strength of 924 ksi was used as a fiber. A 55 : 45 mixture of EPON Resin 825 and Huntsman Jeffamin T-403 was used as a matrix. The composite was wrapped to desired thickness and ori-

entation along the mandrel and then was cured under IR radiation for about 15 minutes while maintaining the rotation of the mandrel to preserve the uniformity of the resin. After this process, the resin was further cured and hardened at a temperature of 250°F for 3 hours. **Testing:** The burst pressure of each of these vessels was tested using a NOVASWISS hand pump system (rated up to 7000 bar). The hand-pump is a hydraulic based hand-pump where pressure can be increased by forcing a fluid into the pressure chamber. Pressure was raised until burst pressure was reached. The rate of increase was about 10 MPa/s. The experimentally observed burst pressure as a function of various composite thicknesses is shown in Figure 4.7. As can be seen, as we increase the composite thickness, the burst pressure does not proportionately increase. Reasons behind this mis-match include the possibility that the assumption of the failure mode to be under hoop stress was violated. As can be seen in Figure 4.7, the failure mode was a more complicated inelastic shear. Another contribution might be due to insufficient bonding between layers of composite.

4.4 High Pressure Micro Valve Design

A valve interface is necessary for controlled release of pressurized fluid. Two different types of valves were realized. One was to release all the pressure during a single operation and other was to continuously release the pressure on demand. The details of each of these efforts are described below.

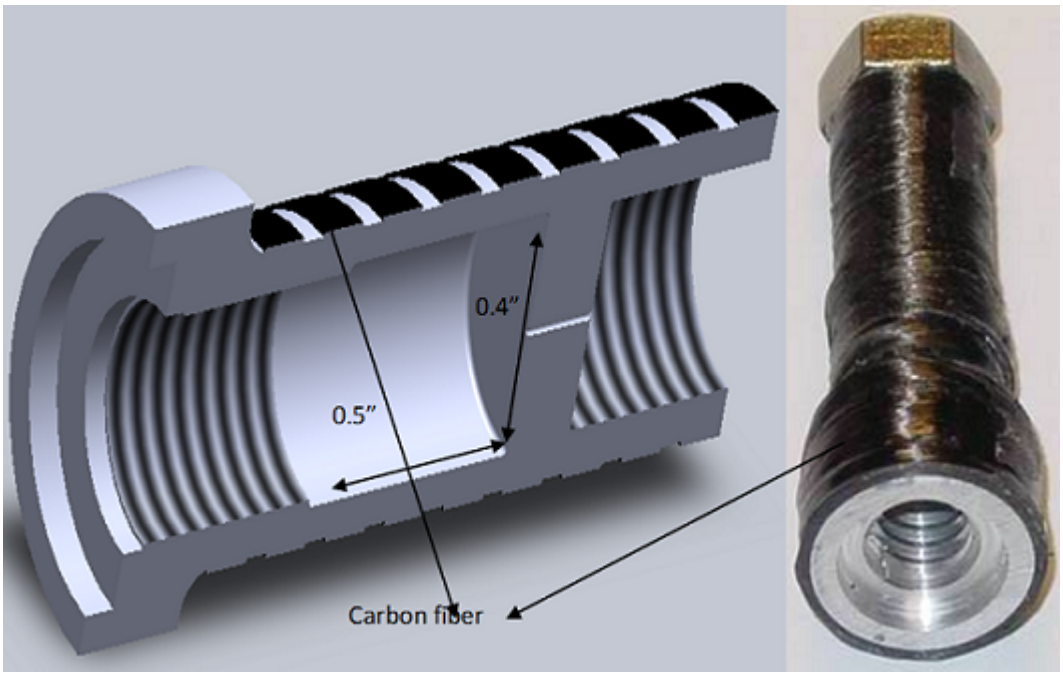

Figure 4.6: Pressure Vessel (a) A schematic cut section of the pressure vessel showing the chamber and wrapping of carbon fiber, (b) A wrapped vessel.

4.4.1 One Shot Valve

One shot valves were manufactured for balloon inflation using CSHPV. The valve was manufactured by drilling a 1 mm diameter hole in the cap of the pressure vessel. A 35 AWG Nichrome wire was placed inside two glass capillaries as shown in Figure 4.8 A and then placed in the 1-mm hole of the cap. Glass capillaries were needed to ensure that the Nichrome wire does not short itself. The hole was then sealed using Cyanoacrylate adhesive. Seal was tested on a hand pump to withstand up to 1600 bars. The valve functions by releasing the pressure by heating the cyanoacrylate seal. Pressure release experiments were performed by trapping dry ice in the vessel. Pressure was released by passing about 1 A of current for about 1 minute. All the pressurized gas was released in about 3.5 minutes. Since the expansion ratio of dry ice is about 554 it places a

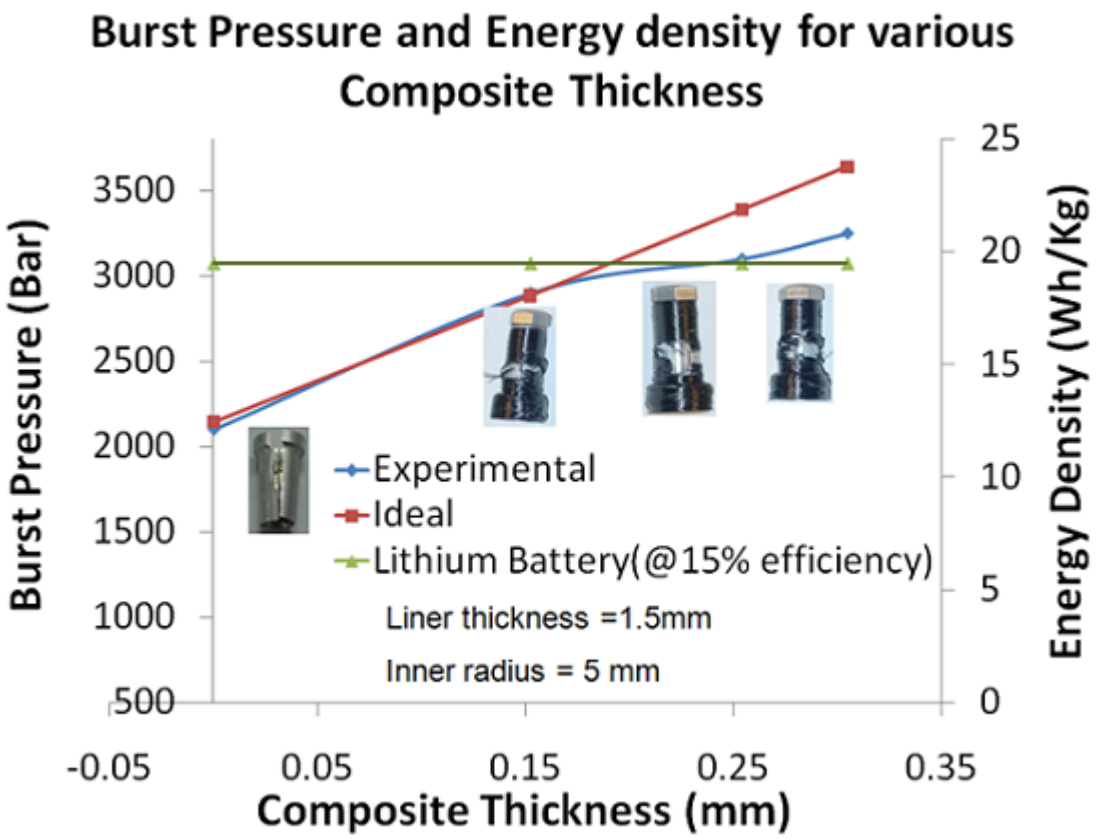

Figure 4.7: Burst pressures obtained for various composite thicknesses and the energy density of the corresponding vessel. The energy density exceeds Lithium batteries at a pressure of 3000 bar.

limit of 554 cc carbon dioxide to be trapped inside the 1-cc vessel so only about 0.5 liters of gas could be inflated in the balloon (Figure 4.8 C) [58]. The system was then released using Nichrome wires that can detach a wooden boom holding the inflation system in place.

4.4.2 Capillary Interface

Flow rates from such high pressure vessels can be significantly high depending on the size of the opening of outlet. Manageable flow rates can be obtained

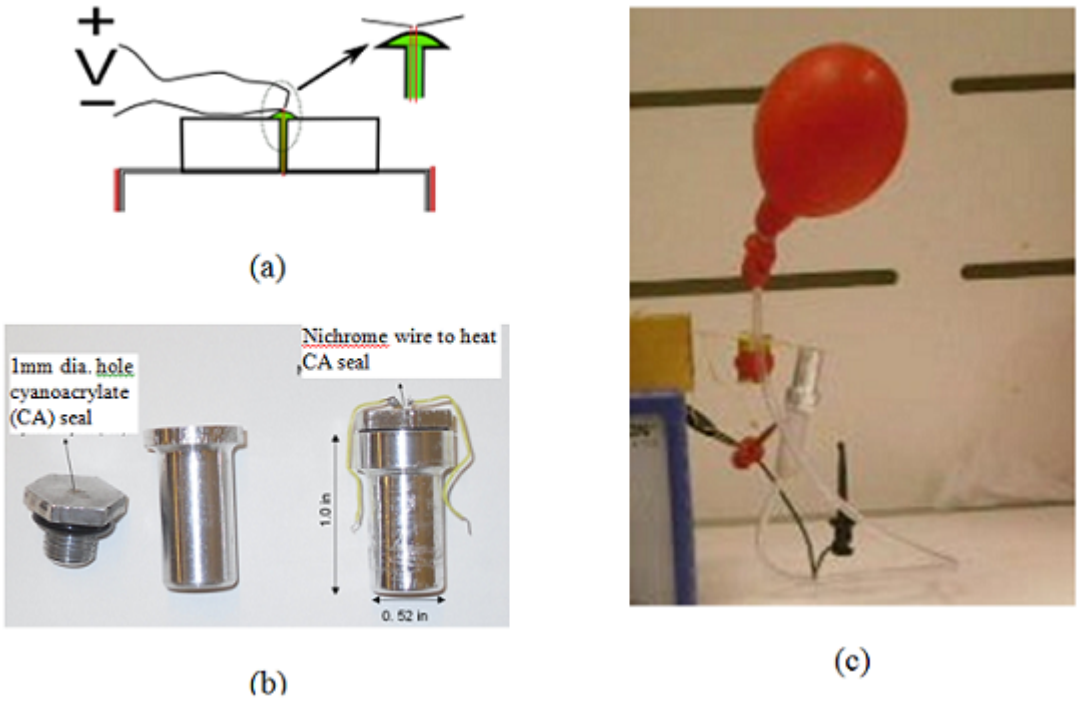

Figure 4.8: (a) Schematic showing principle of the valve i.e. the cyanoacrylate seal and Nichrome wires. (b) A picture of the parts that make up the assembly. (c) Picture of the experimental set up used to inflate a balloon.

by having small size capillaries as an outlet for the flow. These capillaries provide significant resistance to flow and also serve to reduce the force required to regulate airflow. The flow rate through a tube of radius R and length L for compressible flow is proportional to the fourth power of the radius and can be expressed using Hagen-Poiseuille equation as follows:

$$\text{Flow Rate} = \frac{\pi R^4}{16\eta L}\frac{P_i^2 - P_o^2}{P_o} \tag{4.8}$$

where P_o and P_i are the inlet and outlet pressures and η is the kinematic viscosity. Constant flow rates can be obtained with gases that liquefy at high pressure. This is due to the fact that as the gas escapes, it is immediately replaced by evaporating liquid keeping the pressure constant. Carbon dioxide (CO_2) is an example of a gas that liquefies at 70 bar at room temperature which enables the

flow rate to be constant with time. Figure 4.9 shows the plot of flow rate as a function of time for various capillary sizes from a 1-cc vessel holding 1 gram of CO_2. The flow rate decays rapidly after all the liquid CO_2 evaporates. The flow rate as a function of time in this region can be obtained by solving Equation (4.8) and can be obtained as follows:

$$\text{Flow Rate} = \frac{\pi R^2}{16\eta L} P_o \left(\left(\frac{1 + ce^{-kt}}{1 - ce^{-kt}} \right)^2 - 1 \right) \tag{4.9}$$

where c is function exclusively of the initial pressure and k is a function of the geometry of the tube and the gas inside the pressure vessel. Experiments were performed with various capillary sizes to determine the flow rate through various capillary sizes. As can be seen the flow rates obtained match well with the theoretically predicted ones.

4.4.3 Continuous Valve

A microfluidic channel was formed using a micro-drill to incorporate glass-capillaries that provided high resistance so that a small silicon magnetic actuator with hand-wound coil could open and close the flow in continuous or pulsed mode. The capillary was designed to be about 1 m in length winding around the pressure vessel and delivering the gas into a hermetically sealed chamber with a magnetic valve (Figure. 4.10). The Outer diameter of the capillary was 350 microns and was chosen to impart sufficient strength for the capillary to withstand the force from the valve without buckling. The normally-closed valve sealing force was 0.1 $\mu N/\mu m^2/bar$ with 5 - 10 mW of opening power consumption. A rubber elastomer was used to effectively seal the contact between the actuator and the capillary. The pressure vessels were filled with solid CO_2 and sealed.

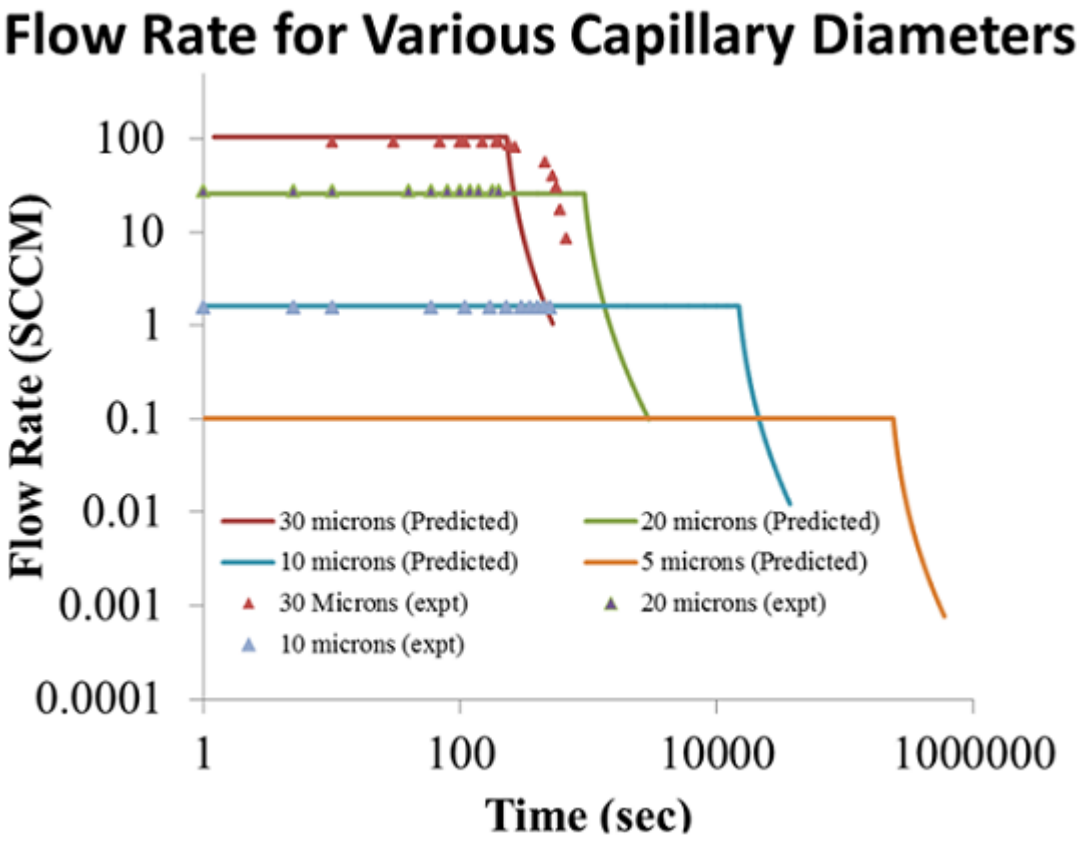

Figure 4.9: Flow rates through capillaries of various sizes.

The pressure vessel maintains a pressure of about 80 bar at room temperature, the liquefaction pressure of liquid CO_2. The flow rate (Figure. 4.9) remains constant till the pressure is above liquefaction pressure as the liquid CO_2 vaporizes to keep the pressure constant, and decreases rapidly after all the liquid CO_2 vaporizes. Energy release is controlled by the capillary microfluidic resistance.

4.5 Applications

Two separate applications of CSHPV were targeted that leverage the miniature size of the pressure vessel. One was to excite a micro motor using air from

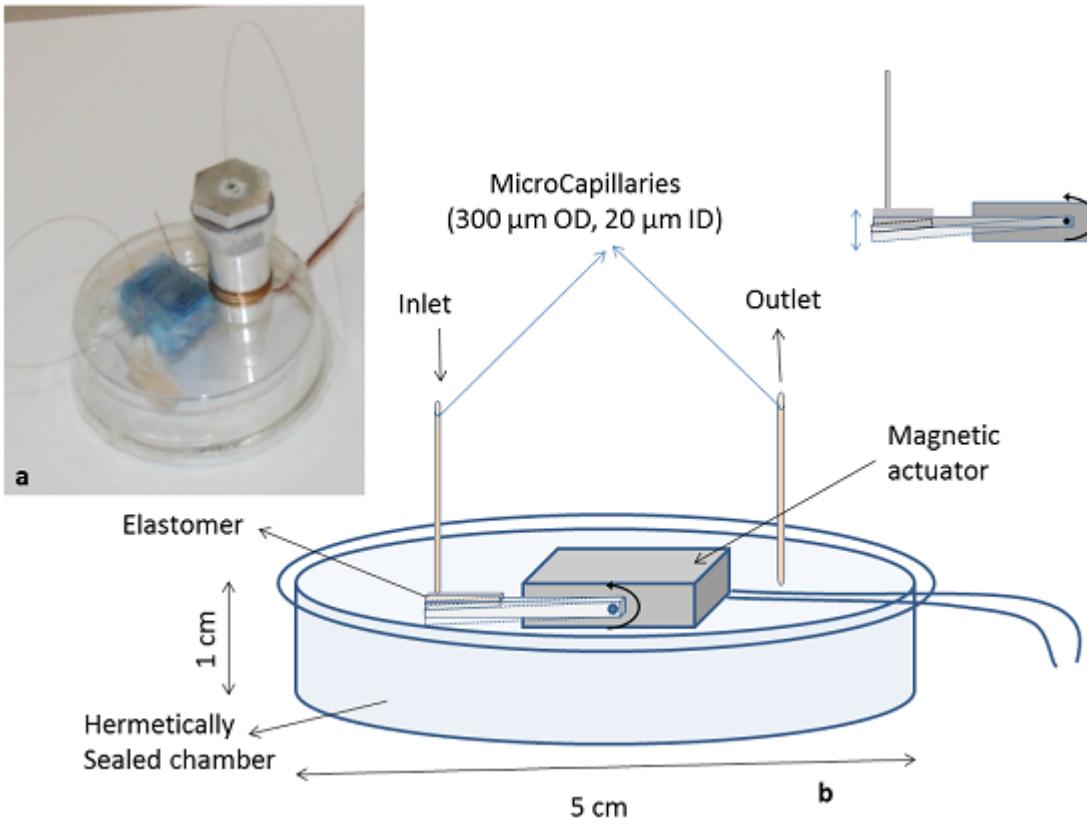

Figure 4.10: (a) Capillary emerging from the pressure vessel and into the hermetically sealed chamber with magnetic actuator for flow control. (b) Enlarged schematic view of the chamber and magnetic valve.

CSHPV with a capillary interface. Another was to use the CSHPV to inflate a pressure cuff wrapped around an arm for blood pressure measurement.

4.5.1 Micromotor Actuation

Air from a CSHPV was directed tangentially onto a MUMPS-fabricated polysilicon surface micromachined rotor (Figure 4.11) [62] leading to rotation of the motor. Using a 5-micron capillary, continuous operation over four days is expected. Using a piezoelectric actuator with a Lithium battery, with a 10 mW

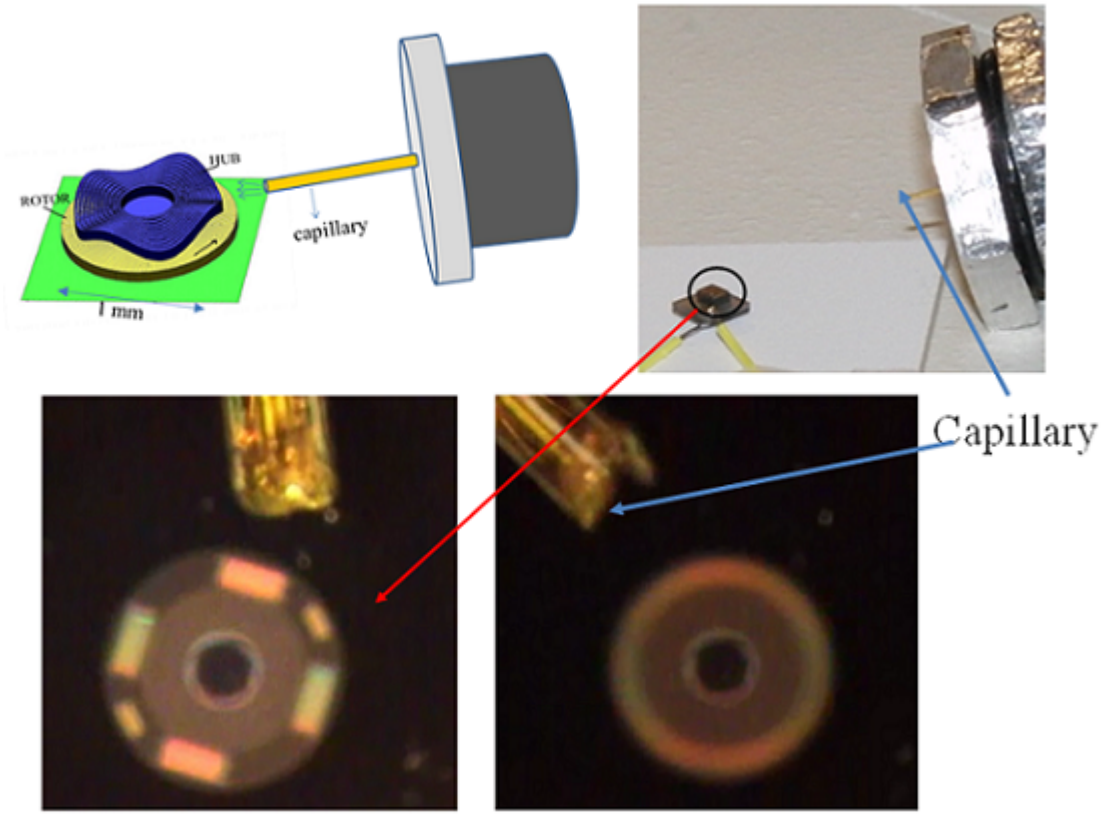

Figure 4.11: Top Left: A schematic showing the principle of working of the motor with pressurized air from the capillary. Top-right: Photograph of a pressure vessel with capillary interface with air being directed on the motor. Bottom: A microscope image showing motor stationary and rotating.

operation would have required a 360 cc Lithium battery.

4.5.2 Inflatable Pressure cuff

CSHPV vessel was used to inflate a pressure cuff in order to examine the potential as a blood pressure sensor. Disposable pressure cuffs were obtained from Welch Allyn . Air from the pressure vessel was released into the Pressure cuff and at the same time, the blood pressure was monitored using a pressure sen-

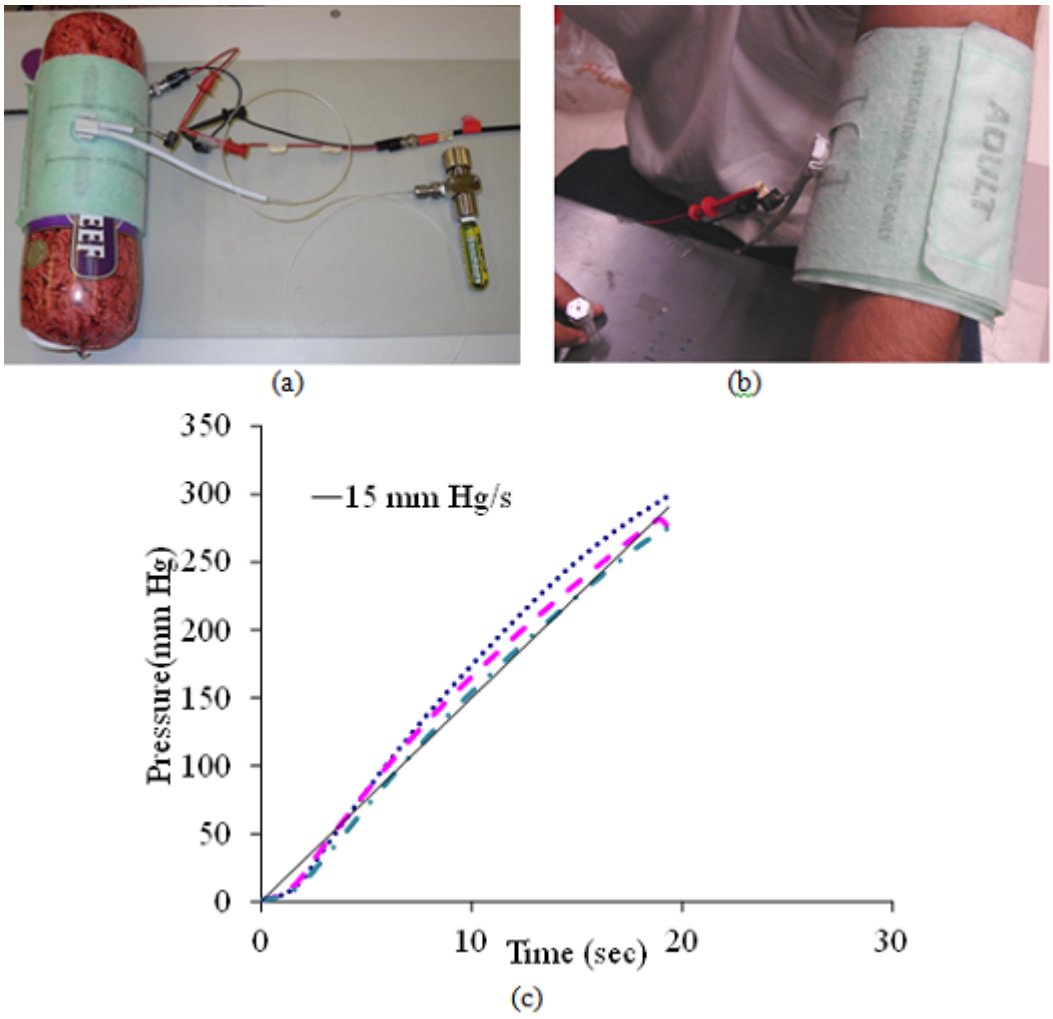

Figure 4.12: (a) Inflatable pressure cuff wrapped around a beef roll to simulate the compressibility of human arm, (b) Pressure cuff wrapped around the human arm, also seen are the pressure vessel and the capillary, (c) Pressure rise rates obtained around a beef roll.

sor (Sensor Amp 15 psi Gage). The set-up and the pressure rise rate are shown in the Figure 4.12. Recommended pressure rise rates of 10-15 mmHg/s were obtained using 20 micron capillaries.

4.6 Conclusion

The technology components for MEMS compatible pneumatic power sources were examined. All the necessary components for long lasting portable pneumatic power source that can be readily integrated with existing fluidic actuators were demonstrated. Over the last 20 years, numerous fluidic actuators have been developed, many with higher force and power density compared to the more common electrostatic, thermal and piezoelectric actuators. Despite these promising properties, pneumatic and hydraulic actuators are still often overlooked in MEMS partly due to the fact that additional elaborate infrastructure is needed to realize full functionality of these actuators. By shrinking the pneumatic power source to a centimeter scale and keeping the energy density comparable to that of Lithium batteries, current work leads us towards realizing the benefit of pneumatic actuators as easily as electrostatic or piezoelectric actuators.

APPENDIX A

COMPRESSED AIR ENERGY DENSITY AND FLOW RATE CALCULATIONS

A.1 Energy Density

The maximum energy that can be obtained from compressed gas is known to be via an isothermal process, where the gas is reversibly expanded keeping the temperature constant. The energy extracted can be given as:

$$W_{A\to B} = \int_{V_A}^{V_B} PdV = \int_{V_A}^{V_B} \frac{nRT}{V} dV = nRT \int_{V_A}^{V_B} \frac{1}{V} dV$$
$$= nRT \ln \frac{V_B}{V_B} = PV \ln \frac{P_A}{P_B}$$

where $P_A V_A = P_B V_B = PV$

A.2 Flow Rate Calculation

The volumetric flow rate of a compressible fluid through a tube is given by Hagen-Poiseuille equation.

$$\Phi = \frac{\pi R^4}{16\eta L}\left(\frac{P_i^2 - P_o^2}{P_o}\right) \tag{A.1}$$

where η is the viscosity of the fluid, P_i is the inlet pressure, P_o is the outlet pressure, L is the length of the tube and R is the radius. When the inlet is a closed system as is the case when all the CO_2 is in gaseous phase, the flow rate

can be related to the inlet pressure drop as:

$$PV = nRT$$

$$\dot{P}V = \frac{\rho\Phi}{M}RT$$

where V is the constant volume of the vessel and M is the Molecular weight of the gas. This results in the following differential equation:

$$\dot{P}_i = \text{Const.}\left(P_i^2 - P_o^2\right)$$

This equation is first order and can be solved fairly easily to give:

$$\Phi = \frac{\pi R^2}{16\eta L}P_o\left(\left(\frac{1 + ce^{-kt}}{1 - ce^{-kt}}\right)^2 - 1\right)$$

APPENDIX B

DETAILS OF BACKPACK

B.1 Components

The backpack with all the components is shown in figure. They are described below:

1. **Actuator:** The actuator was chosen based on power consumption, output torque and the amount of torque the insect would require to rotate the actuator in its equilibrium position. We use a PLANTRACO Smartservo RC-1 Actuator. This actuator provides the benefit output torque and power consumption combination. Several other actuators were also tried, but Smartservo RC1 had better performance.
2. **Battery:** Battery can be chosen depending on the need for flight time and weight. For the longer duration (>15 min) flights, a 3 gram 90 mAh Full River battery could be used. For the shorter duration flights, a 1 gram 30 mAh battery or smaller would suffice.
3. **Receiver:** The actuator mentioned above can be very conveniently actuated with Micro9-S-4CH 1.1 g Servo Rx w/ESC. The receiver weighs 1.1 grams with built in connectors, and could be made potentially lighter without them.
4. **One-way valve:** The oneway valve used was a commercial oneway valve used to inflate Helium from a tank. An 18/12 inch could be attached and inflated. Helium is fed using a tube 2-3 mm in diameter. The valve's

normal input is sealed. The oneway valve is attached to the platform via a bearing to enable free rotation of the platform.

5. **Connecting boom:** We use a balsa wood beam for connecting the moths and act as a platform for the components. We chose a beam about 1 inch wide and 5 inches long with a height of 0.2 cm.

6. **Bearing:** The balloon and the one-way valve are attached to the platform using a bearing to allow free rotation of the beam and not be influenced by the forces experienced by the balloon. The bearing used was from VXB with an ID of 2 mm and OD of 5 mm and a height of 2.3 mm.

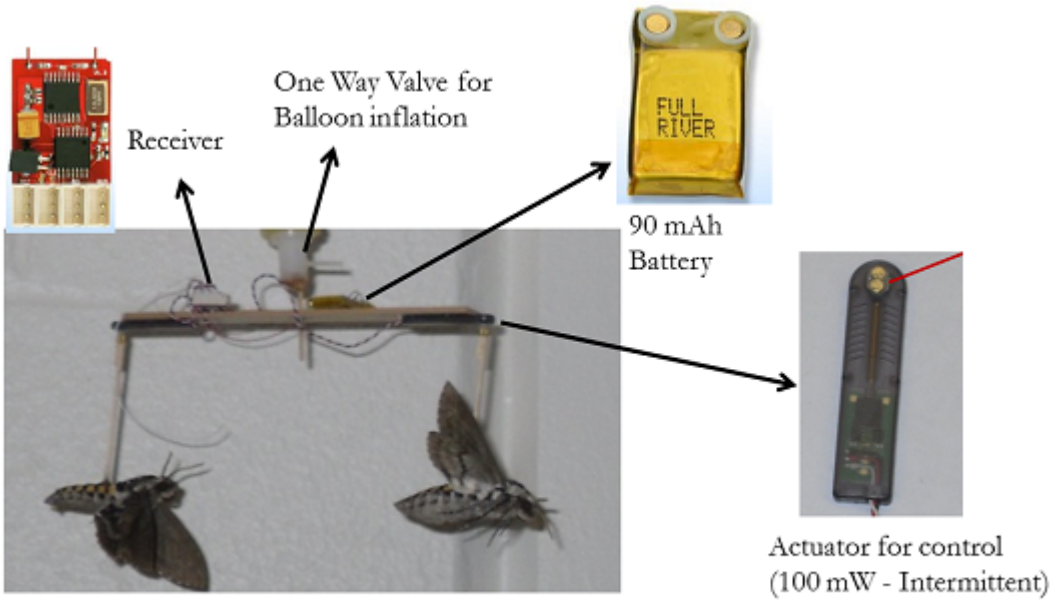

Figure B.1: Figure showing the backpack in an untethered flight experiment with the individual components

B.2 Assembly of the Backpack

In order to assemble a backpack the following procedure was employed. The dual magnets are attached to the actuator using Superglue (CA-40). Similarly dual magnets are attached to balsa sticks that are to be mounted on the back of insects. The bearing was inserted in the connecting beam using 5 minute epoxy. Care should be taken not to let the epoxy enter the balls inside the bearing. A balloon is mounted with its neck snugly fitting the oneway valve and the oneway valve is then attached to the bearing. The actuator is attached to the connecting beam with double sticky tape. Similarly the receiver and the battery are attached to the connecting beam. The Helium is now connected to the oneway valve and the balloon is inflated. Then the insects can be attached to the actuator and untethered flight experiments could be performed B.1.

BIBLIOGRAPHY

[1] C.P. Ellington. The novel aerodynamics of insect flight. *The Journal of Experimental Biology*, 202:3439–3448, 1999.

[2] R.J.Wood. The first takeoff of a biologically-inspired at-scale robotic insect . *IEEE Trans. on Robotics*, 24(2):341–347, 2008.

[3] M.M. O'Meara and T.J.Mueller. Laminar Separation Bubble Characteristics on an Airfoil at Low Reynolds Numbers . *AIAA Journal*, 25(8):1033–1041, 1987.

[4] T. Weis-Fogh. Quick Estimates of Flight Fitness in Hovering Animals, Including Novel Mechanisms for Lift Production . *Journal of Experimental Biology*, 59:169–230, 1973.

[5] T.M. Casey. Flight Energetics of Sphinx Moths: Power Input during Hovering Flight . *Journal of Experimental Biology*, 64:529–543, 1976.

[6] www.delfly.com.

[7] T. Weisfogh. Biology and physics of locust flight. ii. flight performance of the desert locust (schistocerca gregaria). *Philosophical Transactions of the Royal Society of London. Series B, Biological Sciences*, 239:459–510, 1956.

[8] http://www1.eere.energy.gov.

[9] M.H.Dickinson and J.R.B.Lighton. Muscle efficiency and elastic storage in the flight motor of drosophila. *Science*, 268(5207):87–90, 1995.

[10] S.B.Fuller, M.Epstein, S.Waydo, W.B.Dickson, A.D.Straw, M.H.Dickinson, and R.M.Murray. "Flight control in a flapping-wing fruit fly simulator". http://www.ine-news.org/pdf/0050/0050.pdf.

[11] V.Novotny, S.E.Miller, J.Hulcr, R.A.I. Drew, Y. Basset, M.Janda, G.P.Setliff, k.Darrow, A.J.A. Stewart, J.Auga, B.Isua, K.Molem, M.Manumbor, E.Tamtiai, M.Mogia, and G.D.Weiblen. Low beta diversity of herbivorous insects in tropical forests . *Nature*, 448:692–695, 2007.

[12] G.C.McGavin. *Essential Entomology: An order by order introduction.* Oxford University Press, 2001.

[13] H.B.D.Kettlewell. Insect survival and selection for pattern. *Science*, 148(3675):1290–1296, 1965.

[14] M.H.Dickinson, F.O.Lehmann, and S.P.Sane. Wing rotation and aerodynamic basis of insect flight. *Science*, 284(5422):1954–1960, June 1999.

[15] U.Pesavento and Z.J.Wang. Flapping wing flight can save aerodynamic power compared to steady flight. *Physical Review Letters*, 103(11), 2008.

[16] V.B.Wigglesworth. The hormonal regulation of growth and reproduction in insects. *Advances in Insect Physiology*, 2:247–336, 1964.

[17] S.Takeuchi and I.Shimoyama. A radio-telemetry system with a shape memory alloy microelectrode for neural recording of freely moving insects. *IEEE Transactions in Biomedical Engineering*, 51(1):133–137, Jan 2004.

[18] W.E.Green, P.Y P.Y.Oh, and G.Barrows. Flying insect inspired vision for autonomous aerial robot maneuvers in near-earth environments. In *Proceedings of IEEE International Conference on Robotics and Automation(ICRA '04)*, pages 2347–2352, April 2004.

[19] A.Lal and R.F.White. Silicon microfabricated horns for power ultrasonics. In *Proceedings of 8th International Conference on Solid-State Sensors and Actuators, 1995 and Eurosensors IX.. Transducers '95*, pages 405–408, June 1995.

[20] A.Chung and D.Erickson. Engineering insect flight metabolics using immature stage implanted microfluidics. *Lab on a Chip*, 9:669–676, 2009.

[21] R.J.Elzinga. *Fundamentals of Entomology*. Prentice Hall, 1996.

[22] T.Eisner, J.Meinwald, and J.Hildebrand. Bugs, behavior, and biomolecules: the naturalists guide to the future. *Bulletin of Americal Academy of Arts and Sciences*, 1:24–31, 2004.

[23] J.R.Sanes and J.G.Hildebrand. Structure and development of antennae in a moth, manduca sexta. *Developmental Biology*, 51(2):282–299, 1976.

[24] R.H.White, H.Xu, T.A.Munch, R.R.Bennett, and E.A.Grable. The retina of manduca sexta: rhodopsin expression, the mosaic of green-, blue- and uv-sensitive photoreceptors, and regional specialization. *Journal of Experimental Biology*, 206(19):3337–3348, October 2003.

[25] S.N.Fry, N.Rohrseitz, A.D.Straw, and M.H.Dickinson. Trackfly: virtual reality for a behavioral system analysis in free-flying fruit flies. *Journal of Neuroscience Methods*, 171(1):110–117, March 2008.

[26] S.G.Matsumoto and J.G.Hildebrand. Olfactory mechanisms in the moth manduca sexta: response characteristics and morphology of central neurons in the antennal lobes. *Proceedings of the Royal Society of London. Series B, Biological Sciences*, 213(1192):249–277, November 1981.

[27] K.D.Roeder.]: Turning tendency of moths exposed to ultrasound while in stationary flight. *Journal of Insect Physiology*, 13:890–923, 1967.

[28] C.M.William. The juvenile hormone. i. endocrine activity of the corpora allata of the adult. cecropia silkworm. *Biological Bulletin*, 116(2), April 1959.

[29] A.Bozkurt, A.Paul, S.Pulla, A.Ramkumar, B.Blossey, J.Ewer, R.Gilmour, and A.Lal. Microprobe microsystem platform inserted during early metamorphosis to actuate insect flight muscle. In *20th IEEE International Conference on Micro Electro Mechanical Systems (MEMS 2007)*, pages 405–408, January 2007.

[30] I.P.Pavlov. *Conditioned Reflexes: An Investigation of the Physiological Activity of the Cerebral Cortex.* Oxford University Press, 1927.

[31] S.K.Talwar, S.Xu, E.S.Hawley, S.A.Weiss, K.A.Moxon, and J.K.Chapin. Rat navigation guided by remote control. *Nature*, 417:37–38, 2002.

[32] O.Felfoul, E.Aboussouan, A.Chanu, and S.Martel. Real-time positioning and tracking technique for endovascular untethered microrobots propelled by mri gradients. In *Proceedings of International Conference on Robotics and Automation*, 2009.

[33] J.H.Marden. Effects of load-lifting constraints on the mating system of a dance fly. *Ecology*, 70(2):496–502, 1989.

[34] Private discussion with james marden, penn state university.

[35] L.A.Real. Animal choice behaviour and the evolution of cognitive architecture. *Science*, 253:980–986, 1991.

[36] D.C.Sandeman. Angular acceleration, compensatory head movements and

the halteres of flies (lucilia serricata) dc sandeman. *Journal of Comparative Physiology A: Neuroethology*, 136(4):361–367, 1980.

[37] L.P.Tolbert and J.G.Hilderbrand. Organization and synaptic ultrastructure of glomeruli in the antennal lobes of the moth manduca sexta: A study using thin sections and freeze-fracture. *Proceedings Of The Royal Society B*, 213(1192):279–301, 1981.

[38] A.E.Kammer. The motor output during turning flight in a hawkmoth, manduca sexta. *Journal of Insect Physiology*, 17(6):1073–1086, 1971.

[39] www.microflight.com.

[40] www.micromo.com.

[41] S.Pulla and A.Lal. Insect powered micro air vehicles. In *Proceedings of IEEE International Conference on Robotics and Automation, 2009. ICRA '09.*, pages 3657–3662, 2009.

[42] R.J.Wood, S.Avadhanula, M.Menon, and R.S R.S.Fearing. Microrobotics using composite materials: the micromechanical flying insect thorax. In *Proceedings of IEEE International Conference on Robotics and Automation, 2003. ICRA '03.*, pages 1842–1849, 2003.

[43] G.M.Viswanathan, S.V.Buldyrev, S.Havlin, M.G.E.da Luz, E.P.Raposo, and H.E.Stanley. Optimizing the success of random searches. *Nature*, 401:9, 1999.

[44] S.P.Sane, A.Dieudonne, M.A.Willis, and T.L.Daniel. Antennal mechanosensors mediate flight control in moths. *Science*, 315(5813):863–866, 2007.

[45] G.Stange. The ocellar component of flight equilibrium control in dragonflies. *Journal of Comparative Physiology A: Neuroethology, Sensory, Neural, and Behavioral Physiology*, 141(3):335–347, 1981.

[46] L.Ristroph, A.J.Bergou, G.Ristroph, K.Coumes, G.J.Berman, J.Guckenheimer, Z.J.Wang, and I.Cohen. Discovering the flight autostabilizer of fruit flies by inducing aerial stumbles. *Proceeding of National Academy of Sciences (PNAS)*, March 2010.

[47] United States. Dept. of the Army. *Hydrogen generator ML-303/TM and hydrogen generator set AN/TMQ-3*.

[48] R.Z.Sagdeev, V.M.Linkin, J.E.Blamont, and R.A.Preston. The vega venus balloon experiment. *Science*, 231(4744):1407–1408, March 1986.

[49] R.R.Burton. Scott's last expedition: the upper air observations. *Weather*, 61(9), 2006.

[50] C.C.Lim. Indium seals for low-temperature and moderate-pressure applications. *Review of Scientific Instruments*, 57(1):108–114, 1986.

[51] W.Grochala and P.P.Edwards. Thermal decomposition of the non-interstitial hydrides for the storage and production of hydrogen. *Chemical Reviews*, 104(3):1283–1316, 2004.

[52] M.Volder and D.Reynaerts. Pneumatic and hydraulic microactuators: A review. *Journal of Micromechanics and Microengineering*, 20(4), 2010.

[53] O.C.Jeong and S.Konishi. Pneumatic gas regulator with cascaded pdms seal valves. *Sensors Actuators A*, 143:84–89, 2008.

[54] O.C.Jeong and S.Konishi. Fabrication of a peristaltic micro pump with novel cascaded actuators. *Journal of Micromechanics and Microengineering*, 18(2), 2008.

[55] U.Gebhard, H.Hein, E.Just, and P.Ruther. Combination of a fluidic micro-oscillator and micro-actuator in liga-technique for medical application. In *Proceedings of International Conference on Solid State Sensors and Actuators, 1997. TRANSDUCERS '97 Chicago., 1997*, pages 761–764, 1997.

[56] M.Volder, F.Ceysses, D.Reynaerts, and R.Puers. Microsized piston-cylinder pneumatic and hydraulic actuators fabricated by lithography. *IEEE Journal of Micro ElectroMechanical Systems (MEMS)*, 18:1100–1104, 2009.

[57] S.Yokota, K.Kawamura, K.Takemura, and K.Edamura. A high integration micro-motor using electro-conjugated fluid (ecf). *Journal of Robotics and Mechatronics*, 17:142–148, 2005.

[58] Y.Mita, S.Konishi, and H.Fujita. Two dimensional micro conveyance system with through holes for electrical and fluidic interconnection. In *Proceedings of International Conference on Solid State Sensors and Actuators, 1997. TRANSDUCERS '97 Chicago., 1997*, pages 37–40, 1997.

[59] http://www.toraycfa.com/pdfs/T1000GDataSheet.pdf.

[60] A.K.Law. *Mechanics of Composite Materials*. CRC, 2005.

[61] S.T.Peters, W.D.Humphrey, and R.F.Foral. *Filament winding composite structure fabrication*. SAMPE International Business Office, 2 edition, 2000.

[62] http://www.kaiseraluminum.com/wp-content/themes/kac/files/alloy-pdfs/.